# Physics of automated-driving vehicular traffic

Boris S. Kerner
*Physics of Transport and Traffic, University of Duisburg-Essen, 47048 Duisburg, Germany*

(Received 27 March 2023; accepted 7 June 2023; published 6 July 2023)

We have found that phase transitions occurring between three traffic phases [free flow (F), synchronized flow (S), and wide moving jam (J)] determine the spatiotemporal dynamics of traffic consisting of 100% automated-driving vehicles moving on a two-lane road with an on-ramp bottleneck. This means that three-phase traffic theory is a common framework for the description of traffic states independent of whether human-driving or automated-driving vehicles move in vehicular traffic. To prove this, we have studied automated-driving vehicular traffic with the use of classical Helly's model [*Proceedings of the Symposium on Theory of Traffic Flow* (Elsevier, Amsterdam, 1959), pp. 207–238] widely applied for automated vehicle motion. Although dynamic rules of the motion of automated-driving vehicles in a road lane are qualitatively different from those of human-driving vehicles, we have revealed that traffic breakdown (F → S transition) at the bottleneck exhibits the nucleation nature, which was observed in empirical field data measured in traffic consisting of 100% human-driving vehicles. The physics of the nucleation nature of the F → S transition in automated-driving traffic is associated with a discontinuity in the rate of lane-changing that causes the discontinuity in the rate of over-acceleration. This discontinuous character of over-acceleration leads to both the existence and self-maintaining of synchronized flow at the bottleneck in automated-driving vehicular traffic as well as to the existence at any time instant of a range of highway capacities between some minimum and maximum capacities. Within the capacity range, an F → S transition can be induced; however, when the maximum capacity is exceeded, then after some time-delay a spontaneous F → S transition occurs at the bottleneck. The phases F, S, and J can coexist each other in space and time.

DOI: 10.1103/PhysRevE.108.014302

## I. INTRODUCTION

In traffic of human-driving vehicles, traffic breakdown that is a transition from free flow to congested traffic occurs mostly at bottlenecks. Already in 1950s–1960s two classes of models for traffic breakdown were introduced:

(i) In the classical Lighthill-Whitham-Richards (LWR) model [1,2], it is assumed that there is a fundamental diagram for traffic flow at a highway bottleneck; the maximum flow rate at the fundamental diagram is equal to highway capacity: If the flow rate upstream of a bottleneck exceeds the capacity, then traffic breakdown occurs; otherwise, no traffic breakdown can occur at the bottleneck (see, e.g., Refs. [3–7]).

(ii) In 1958, Herman, Gazis, Montroll, Potts, Rothery, and Chandler from General Motors (GM) Company [8–11] as well as by Kometani and Sasaki [12–15] assumed that traffic breakdown occurs due to traffic flow instability in vehicular traffic. This classical traffic instability was incorporated into a number of traffic flow models (e.g., papers, reviews, and books [6,7,16–33]). As found in Ref. [34], the classic traffic instability leads to a phase transition from free flow (F) to a wide moving jam (J) called an F → J transition.

It is commonly assumed that in future vehicular traffic automated-driving vehicles [automated vehicle (AV)] will play a decisive role (see, e.g., Refs. [35–49]). Automated-driving is realized through the use of an automated system in a vehicle that controls over the vehicle in traffic flow as well as through the use of cooperative driving realized through vehicle-to-vehicle communication or/and through vehicle-to-infrastructure communication (see, e.g., Refs. [50–54]). Currently, there are many different scientific directions in which a variety of theoretical questions about mixed traffic consisting of a random distribution of automated-driving and human-driving vehicles should be answered. To the questions belong, for example, the question about the effect of automated vehicles on highway capacity, traffic breakdown as well as other traffic characteristics (e.g., Refs. [55–96]), what environmental impacts of automated vehicles on mixed traffic can be expected (e.g., see a review in Ref. [97]), or how different social dilemmas arising in mixed traffic can be solved (e.g., Refs. [98,99]).

It should be noted that in most theoretical studies of the effect of automated vehicles on mixed traffic (e.g., see Refs. [55–94]), motion of human-driving vehicles is described with the use of the above-mentioned standard traffic flow models [1–33].

However, from a study of empirical field traffic data it was found that real traffic breakdown is a transition from free flow (F) to synchronized flow (S) called an F → S transition that occurs in metastable free flow with respect to the F → S transition at a bottleneck [100–102] (see, for a review, Refs. [103–107]): The F → S transition (traffic breakdown) exhibits the empirical nucleation nature (Fig. 1). The LWR theory [1–7] cannot explain the nucleation nature of real traffic breakdown. The classical traffic instability [6–34] that

 

leads to the F → J transition [21–24,27,34] cannot also explain real traffic breakdown at highway bottlenecks.[1]

To explain the empirical nucleation nature of traffic breakdown (F → S transition), the author introduced three-phase traffic theory [100–107]). The three-phase traffic theory is a framework for the description of empirical traffic data in three phases: Free flow (F), synchronized flow (S) and wide moving jam (J); the traffic phases S and J belong to congested traffic. The first implementations of the three-phase traffic theory in mathematical traffic flow models have been made in [110,111]. These stochastic models have been further developed for different applications (see, e.g., Ref. [112]). Over time, other traffic flow models, which incorporate hypotheses of the three-phases traffic theory, have also been developed (see, e.g., Refs. [113–135]). With the use of a microscopic three-phase traffic model for human-driving vehicles, the effect of a small share of automated vehicles on traffic breakdown in mixed traffic at bottlenecks has been studied in Ref. [136].

A basic hypothesis of the three-phase traffic theory is that in some traffic situations vehicle acceleration called *over-acceleration* exhibits a *discontinuous character* (Fig. 2): In synchronized flow, the probability of over-acceleration is considerably lower than it is in free flow [100,101,103].[2] It has been shown that the discontinuous character of over-acceleration causes a metastability of free flow with respect to the F → S transition; in its turn, this metastability explains the empirical nucleation nature of traffic breakdown observed in measured field traffic data. The three-phase traffic theory has been initially created for the description of empirical *human-driving* vehicular traffic [100–106].

The objective of this paper is to show that the spatiotemporal dynamics of traffic consisting of 100% automated-driving vehicles is described in the framework of three-phase traffic theory. It should be emphasized that dynamic rules of motion of automated vehicles in a road lane can be developed that are totally different from the real dynamic behavior of human-driving vehicles. Therefore, a question can arise:

– Why should the three-phase traffic theory describe spatiotemporal phase transitions in traffic flow consisting of 100% of automated vehicles whose dynamics rules of motion in road lane can be totally different from the real dynamic behavior of human-driving vehicles?

To answer this question, we should recall that one of the mechanisms of over-acceleration exhibiting the discontinuous character (Fig. 2) is vehicle acceleration through lane-changing to a faster lane on a multi-lane road [100,101,103].[3] Either a human-driving or automated-driving vehicle changes to a neighborhood target lane if (i) some *incentive conditions* for lane-changing (like the vehicle can pass the preceding vehicle or/and move faster in the target lane) *and* (ii) some *safety conditions* for lane-changing are satisfied, at which no collisions between vehicles can occur. Thus, if the discontinuous character of over-acceleration due to lane-changing to

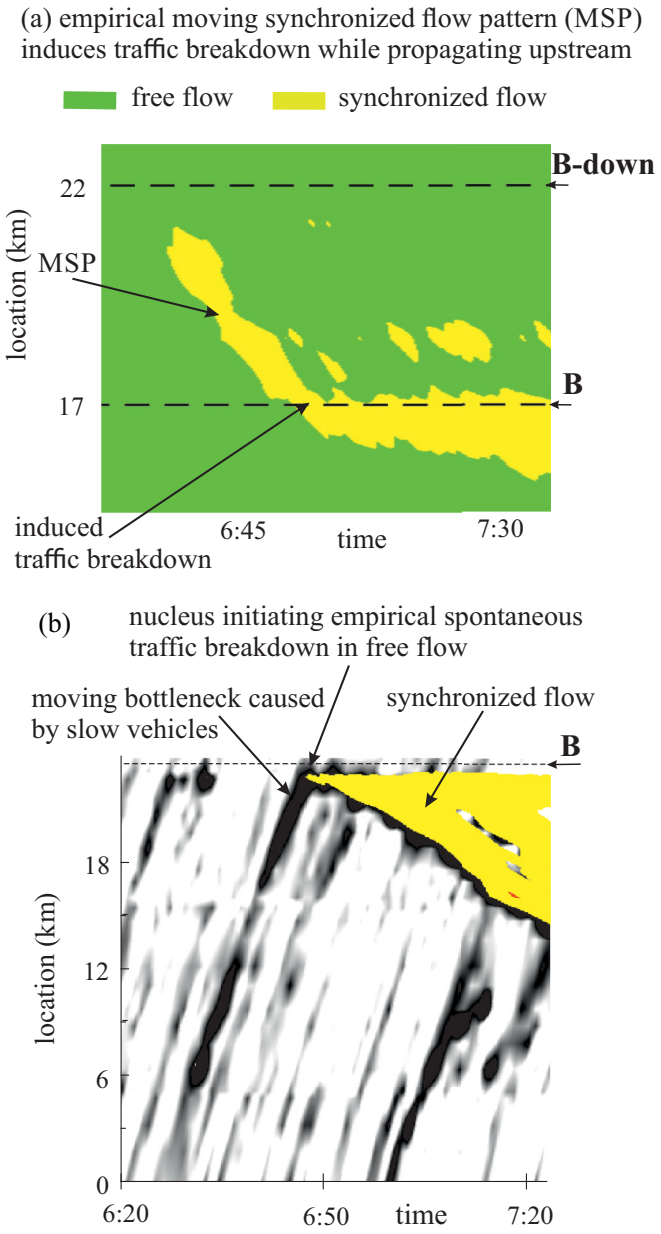


FIG. 1. Empirical nucleation nature of traffic breakdown (F → S transition) at bottlenecks in human-driving vehicular traffic; traffic data were measured with road detectors installed along road sections [100,101,103,108]: (a) Speed data in space and time presented with averaging method of [109]: A moving synchronized flow pattern (MSP) that has emerged at downstream bottleneck (B-down) while propagating upstream induces F → S transition (induced traffic breakdown) at upstream on-ramp bottleneck (B). (b) One of the empirical waves (black colored waves) of decrease in the average speed caused by slow moving vehicles (moving bottleneck) while propagating downstream in free flow acts as a nucleus for spontaneous F → S transition (spontaneous traffic breakdown) at bottleneck (B) when the speed wave propagates through the bottleneck. Adapted from Ref. [106].

[1]In more details, this criticism of standard traffic models can be found in books [103–106]; in particular, see Appendix C in Ref. [106].

[2]See explanations of the term *over-acceleration* in Sec. 8.1.5 of Ref. [106].

[3]In Refs. [100,101,103], the probability of over-acceleration shown in Fig. 2(a) has been called "probability of passing" (see Fig. 5.7(b) of Ref. [103]).

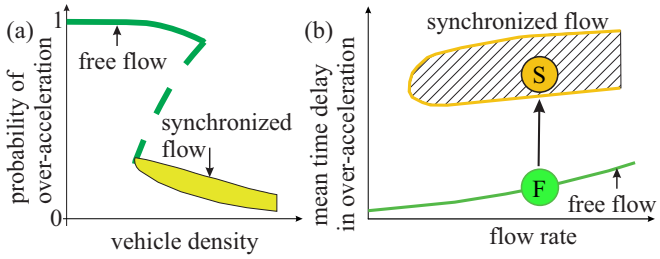


FIG. 2. Discontinuous character of over-acceleration [100,101,103]: (a) Qualitative presentation of over-acceleration probability during a given time interval. Equivalent presentation of (a) as a discontinuous dependence of the mean time delay in over-acceleration on the flow rate; F and S are states of free flow and synchronized flow, respectively. Adapted from Refs. [103,106].

a faster lane (Fig. 2) is realized for human-driving vehicles, it should be also for automated vehicles: The discontinuous character of over-acceleration can be assumed to be an universal physical feature of vehicular traffic.

The paper is organized as follows: In Sec. II, we consider a microscopic model of automated-driving vehicular traffic on a two-lane road and study the physics of the nucleation nature of the F → S transition at a bottleneck. The existence of a range of highway capacities at any time instant is the subject of Sec. III. In Sec. IV, a generalization of nucleation features of the F → S transition in automated-driving traffic is made. Transitions between the three phases F, S, and J in automated-driving traffic are studied in Sec. V. In Discussion (Sec. VI), we show that the basic result about the nucleation nature of the F → S transition at the bottleneck remains for string-unstable automated-driving traffic and even if a different model for automated-driving vehicles is used.

## II. PHYSICS OF METASTABILITY OF AUTOMATED-DRIVING VEHICULAR TRAFFIC AT BOTTLENECK WITH RESPECT TO F → S TRANSITION

### A. Model of automated-driving vehicular traffic on two-lane road with on-ramp bottleneck

We study a model of vehicular traffic consisting of 100% identical automated vehicles moving on a two-lane road with an on-ramp bottleneck. We assume that the control over an automated vehicle moving in a road lane is realized through an adaptive cruise control system (ACC) that is described by a classical model in which the acceleration (deceleration) $a$ of the automated vehicle is determined by the space gap to the preceding vehicle $g = x_\ell - x - d$ and the relative speed $\Delta v = v_\ell - v$ measured by the automated vehicle as well as by some optimal space gap $g_{\rm opt}$ between the automated vehicle and the preceding automated vehicle (see, e.g., Refs. [36–40,46–48]):

$$a = K_1(g - g_{\rm opt}) + K_2\Delta v, \tag{1}$$

where $x$ and $v$ are the coordinate and the speed of the automated vehicle, $x_\ell$ and $v_\ell$ are the coordinate and the speed of the preceding automated vehicle, $d$ is the vehicle length; here and below $v$, $v_\ell$, and $g$ are time-functions; $K_1$ and $K_2$ are constant coefficients of automated vehicle adaptation;

$$g_{\rm opt} = v\tau_{\rm d}, \tag{2}$$

$\tau_{\rm d}$ is a desired time headway of the automated vehicle to the preceding automated vehicle. The classical model (1), (2) that is currently used in most studied of automated-driving in a road lane [36–40,46–48] is related to Helly's car-following model [137]. The motion of the automated vehicle in a road lane is found under conditions $0 \leqslant v \leqslant v_{\rm free}$ from the solution of equations[4] $dv/dt = a$, $dx/dt = v$, where the maximum speed (in free flow) $v_{\rm free}$ is a constant. There can be string instability of a long enough platoon of automated vehicles (1), (2) [36–40,46–48]. As found by Liang and Peng [38], coefficients $K_2$ and $K_1$ in Eq. (1) can be chosen to satisfy condition for string stability

$$K_2 > \left(2 - K_1\tau_{\rm d}^2\right)/2\tau_{\rm d}. \tag{3}$$

In the main text of the paper (Secs. II–V), we consider only automated vehicles whose parameters satisfy condition (3) for string stability.[5]

We use incentive lane changing rules from the right to left lane R → L (4) and from the left to right lane L → R (5) as well as safety conditions (6) known for human-driving vehicles (see, e.g., Ref. [138])

$$R \to L: v^+(t) \geqslant v_\ell(t) + \delta_1 \text{ and } v(t) \geqslant v_\ell(t), \tag{4}$$

$$L \to R: v^+(t) \geqslant v_\ell(t) + \delta_2 \text{ or } v^+(t) \geqslant v(t) + \delta_2, \tag{5}$$

$$g^+(t) \geqslant v(t)\tau_2, \quad g^-(t) \geqslant v^-(t)\tau_1, \tag{6}$$

at which the automated vehicle changes to the faster target lane with the objective to pass a slower automated vehicle in the current lane if time headway to preceding and following vehicles in the target lane are not shorter than some given safety time headway $\tau_1$ and $\tau_2$. In Eqs. (4)–(6), superscripts $+$ and $-$ denote, respectively, the preceding and the following vehicles in the target lane; $\tau_1$, $\tau_2$, $\delta_1$, $\delta_2$ are positive constants.[6]

Open boundary conditions are applied. At the beginning of the two-lane road $x = 0$ vehicles are generated one after another in each of the lanes of the road at time instants $t^{(k)} = k\tau_{\rm in}$, $k = 1, 2, \ldots$, where $\tau_{\rm in} = 1/q_{\rm in}$, $q_{\rm in}$ is a given

[4]These equations are solved with the second-order Runge-Kutta method with time step $10^{-2}$. No noticeable changes in simulation results have been found when time step of calculation has been reduced to $10^{-3}$ s.

[5]The exception is a discussion in Sec. VI A, in which we compare traffic phenomena at the bottleneck under string-stability condition (3) studied in Secs. II–V with traffic phenomena occurring in free flow at the same bottleneck, when automated vehicles do not satisfy condition for string stability (3).

[6]It should be noted that in Eqs. (4) and (5) the value $v^+$ at $g^+ > L_{\rm a}$ and the value $v_\ell$ at $g > L_{\rm a}$ are replaced by $\infty$, where $L_{\rm a}$ is a look-ahead distance; in simulations, we have used $L_{\rm a} = 80$ m. However, due to large flow rates used in simulations both condition $g^+ > L_{\rm a}$ and condition $g > L_{\rm a}$ are not satisfied. The exception is the case of a moving bottleneck (MB) in automated-driving vehicular traffic that is considered in Sec. II F.

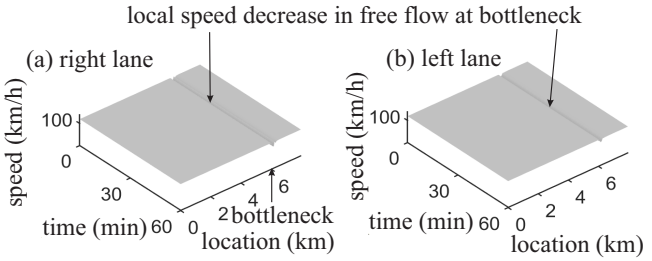


FIG. 3. Simulations with model of Sec. II A of the occurrence of local speed decrease in free flow on two-lane road at bottleneck: Speed in space and time in the right lane (a) and left lane (b). $q_{\text{in}} = 2571$ (vehicles/h)/lane, $q_{\text{on}} = 720$ vehicles/h. Parameters of automated vehicles: $\tau_{\text{d}} = 1$ s, $K_1 = 0.3$ s$^{-2}$, $K_2 = 0.9$ s$^{-1}$, $v_{\text{free}} = 120$ km/h, $d = 7.5$ m. Lane-changing parameters: $\delta_1 = 1$ m/s, $\delta_2 = 5$ m/s, $\tau_1 = 0.6$ s, $\tau_2 = 0.2$ s. Road and on-ramp parameters: road length $L = 8$ km, $x_{\text{on}} = 6$ km, $L_{\text{m}} = 0.3$ km, $\lambda_{\text{b}} = 0.3$ s.

time-independent flow rate per road lane. The initial vehicle speed is equal to $v_{\text{free}}$. After a vehicle has reached the end of the road $x = L$ it is removed. Before this occurs, the farthest downstream vehicle maintains its speed and lane.

In the on-ramp model, there is a merging region of length $L_{\text{m}}$ in the right road lane that begins at road location $x = x_{\text{on}}$ within which automated vehicles can merge from the on-ramp. Vehicles are generated at the on-ramp one after another at time instants $t^{(m)} = m\tau_{\text{on}}, m = 1, 2, \ldots$, where $\tau_{\text{on}} = 1/q_{\text{on}}$, $q_{\text{on}}$ is the on-ramp inflow rate. To reduce a local speed decrease occurring through the vehicle merging at the on-ramp bottleneck, as assumed for many known cooperative automated driving scenarios, automated vehicles merge with the speed of the preceding vehicle $v^+$ at a middle location $x = (x^+ + x^-)/2$ between the preceding and following vehicles in the right lane, when the space gap between the vehicles exceeds some safety value $g_{\text{target}}^{(\min)} = \lambda_{\text{b}} v^+ + d$, i.e., some safety condition $x^+ - x^- - d > g_{\text{target}}^{(\min)}$ should be satisfied. In accordance with these merging conditions, the space gap for a vehicle merging between each pair of consecutive vehicles in the right road lane is checked, starting from the upstream boundary of the merging region. If there is such a pair of consecutive vehicles, the vehicle merges onto the right road lane; if there is no pair of consecutive vehicles, for which the safety condition is satisfied at the current time step, the procedure is repeated at the next time step, and so on.

When free flow is realized at the bottleneck, we have found a known result that due to R → L lane-changing the on-ramp inflow is distributed between two lanes that causes the occurrence of local speed decrease in both the right and left road lanes at the bottleneck (Fig. 3).[7]

### B. Free flow metastability at bottleneck

As mentioned, rules of vehicle motion of Sec. II A as well as the occurrence of local speed decrease in both road lanes at the bottleneck in free flow are known in vehicular traffic theory. Nevertheless, we have revealed that the free-flow state at the bottleneck shown in Fig. 3 is in a metastable state with respect to an F → S transition.

To prove this result, at a time instant $T_{\text{ind}}$ we have disturbed the free-flow state at the bottleneck shown in Fig. 3 through the application of a time-limited on-ramp inflow impulse $\Delta q_{\text{on}}$ of some duration $\Delta t$ (Fig. 4): (i) At time interval $0 \leqslant t < T_{\text{ind}}$, the on-ramp inflow rate $q_{\text{on}}$ is the same as that in Fig. 3 and, therefore, the same free-flow state is realized; (ii) during the impulse $T_{\text{ind}} \leqslant t \leqslant T_{\text{ind}} + \Delta t$ the on-ramp inflow rate has increased to a large enough value $q_{\text{on}} + \Delta q_{\text{on}}$ at which traffic congestion is realized at the bottleneck; (iii) at time $t > T_{\text{ind}} + \Delta t$, although the on-ramp inflow rate has reduced to its initial value $q_{\text{on}}$, rather the free-flow state returns at the bottleneck, congested traffic persists at the bottleneck. The downstream front of induced congested traffic is fixed at the bottleneck while the upstream front of congested traffic is continuously propagate upstream (Fig. 4). In accordance with the phase definitions made in three-phase traffic theory [103], the induced congested traffic belongs to the synchronized flow phase of automated-driving vehicular traffic. Thus, at the same on-ramp inflow rate $q_{\text{on}}$ there can be either a free-flow state or a synchronized flow state at the bottleneck, i.e., free flow in Fig. 3 is indeed in a metastable state with respect to an F → S transition at the bottleneck.

### C. Discontinuity in the rate of over-acceleration through lane-changing

To explain the physics of the free-flow metastability with respect to the F → S transition (Sec. II D), we should first explain here that there is a *discontinuity* in the rate of R → L lane-changing denoted by[8] $R_{\text{RL}}$. The discontinuity in the rate

[7]To explain the occurrence of local speed decrease in free flow in the both road lanes (Fig. 3), we should note that there is an asymmetry between the lanes. The physical cause of the asymmetry between the left and right lanes on the road is the on-ramp bottleneck. Indeed, in free-flow vehicles that merge from the on-ramp onto the right lane cause a local speed decrease in the right lane. Vehicles moving in the right lane should decelerate while approaching the local speed decrease. For this reason, these vehicles try to change to the left lane in which the speed is higher. Rule (4) determines conditions for this R → L lane-changing. Contrary to the local speed decrease in the right lane that occurs due to the bottleneck, without R → L lane-changing there is no local speed decrease in free flow in the left lane. The R → L lane-changing ensures a distribution of the on-ramp inflow between road lanes and, therefore, the R → L lane-changing results in the occurrence of a local speed decrease in the left lane, as shown in Fig. 3(b). As found in simulations presented in the paper below, due to the above-mentioned asymmetry between the left and right lanes, within the local speed decrease the minimum vehicle speed in the left lane is higher than in the right lane. For this reason, a return L → R lane-changing from the left lane to the right lane governed by rule (5) does not occur even if in (4) and (5) values $\delta_1 = \delta_2$ [see Fig. 23(a)]. The exception is the model of a moving bottleneck (MB) in automated-driving vehicular traffic: downstream of the MB a return L → R lane-changing can occur, as shown in Figs. 14(a) and 14(b).

[8]$R_{\text{RL}}$ is the number of automated vehicles that change from the right lane to the left lane during a time unit within the road region $x_{\text{on}} - L_{\text{RL}} \leqslant x \leqslant x_{\text{on}} + L_{\text{m}}$, where parameter $L_{\text{RL}} = 0.06$–$0.1$ km used in simulations should guarantee that R → L lane-changing at the

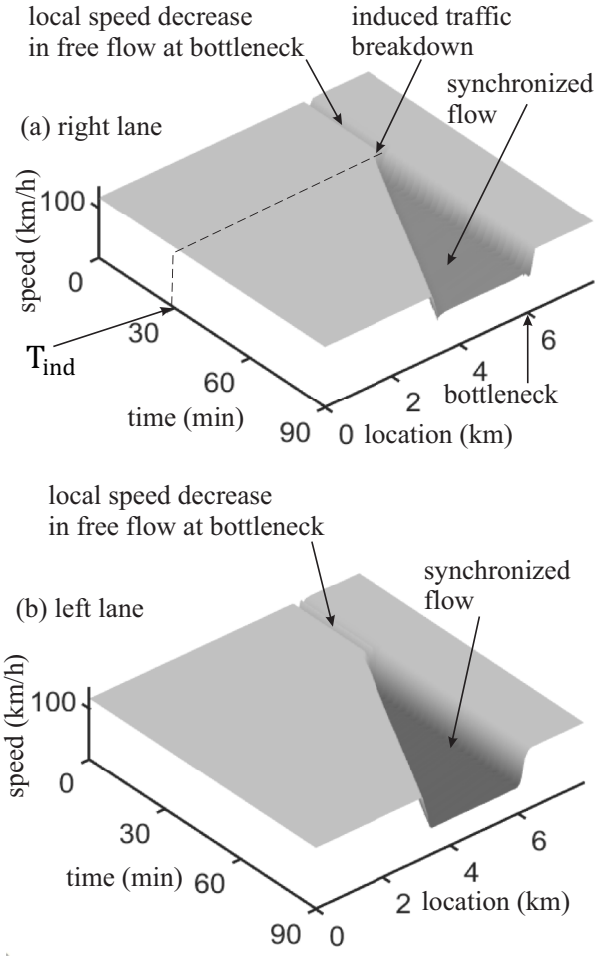


FIG. 4. Proof of the metastability of free-flow state shown in Fig. 3 in automated-driving vehicular traffic moving on two-lane road with bottleneck: Speed in space and time in the right lane (a) and left lane (b). Parameters of on-ramp inflow-rate impulse inducing F → S transition at bottleneck: $T_{ind} = 30$ min, $\Delta q_{on} = 180$ vehicles/h, $\Delta t = 2$ min. Other model parameters are the same as those in Fig. 3.

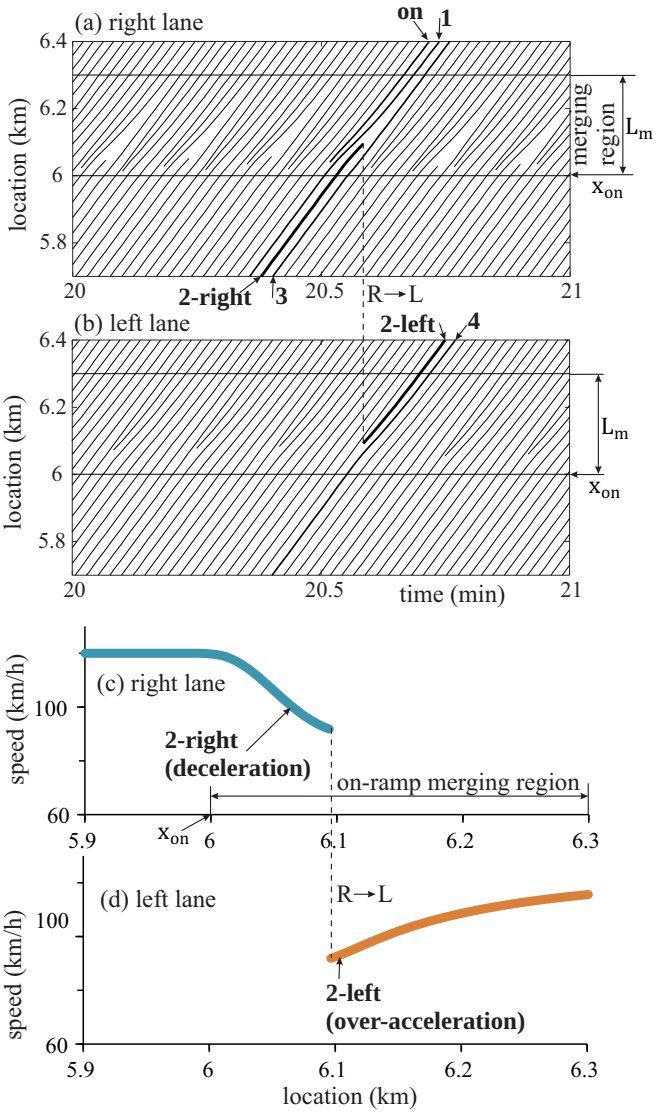


FIG. 5. Continuation of Figs. 3 and 4. (a), (b) Simulated vehicle trajectories within local speed decrease in free flow at bottleneck in the right lane (a) and left lane (b) at time $t < T_{ind}$. (c), (d) Location-functions of speed of vehicle 2 labeled by "2-right" in the right lane (c) and by "2-left" in left lane (d) in panels (a), (b). R → L lane-changing of vehicle 2 is marked by dashed vertical lines R → L.

of R → L lane-changing is realized due to the F → S transition, i.e., when free flow transforms into synchronized flow. Examples of R → L lane-changing in free flow and synchronized flow are shown, respectively, in Figs. 5 and 6 through the use of dashed vertical lines R → L.[9] In free flow occurring during time $0 \leqslant t < T_{ind}$, we have found $R_{RL} \approx 6.1\,\text{min}^{-1}$, whereas in synchronized flow that occurs at the bottleneck at $t \geqslant T_{ind}$, we have found that R → L lane-changing rate $R_{RL}$ reduces sharply to $R_{RL} \approx 2.8\,\text{min}^{-1}$ [Fig. 7(a)]. To explain the abrupt reduction of the rate of R → L lane-changing $R_{RL}$ occurring due to the F → S transition, we mention that in synchronized flow the mean time headway between vehicles $\tau_{mean}^{(syn)}$ reduces while becoming close to $\tau_d = 1$ s. At this short

upstream front of synchronized flow (after the F → S transition has occurred) does not come in the calculation of $R_{RL}$. Indeed, when synchronized flow is at the bottleneck, then only R → L lane-changing at the downstream front of synchronized flow are responsible for the discontinuous character of over-acceleration that leads to the nucleation natures of the F → S transition at the bottleneck. Contrarily, as we show in Sec. II E 1, there is another effect of R → L lane-changing occurring at the upstream front of synchronized flow. This effect of R → L lane-changing causes the synchronization of the velocities of the upstream fronts of synchronized flow in the right and left lanes.

[9]We should note that the on-ramp merging region in Figs. 5 and 6 exists in the right lane *only* [labeled by "merging region" in Figs. 5(a) and 6(a)]. The use of labels "$x_{on}$" and "$L_m$" in Figs. 5(b) and 6(b) (as well as in some other figures below) for the left lane should emphasize that R → L lane-changing resulting in the discontinuous character of over-acceleration occurs in the vicinity of the on-ramp merging region.

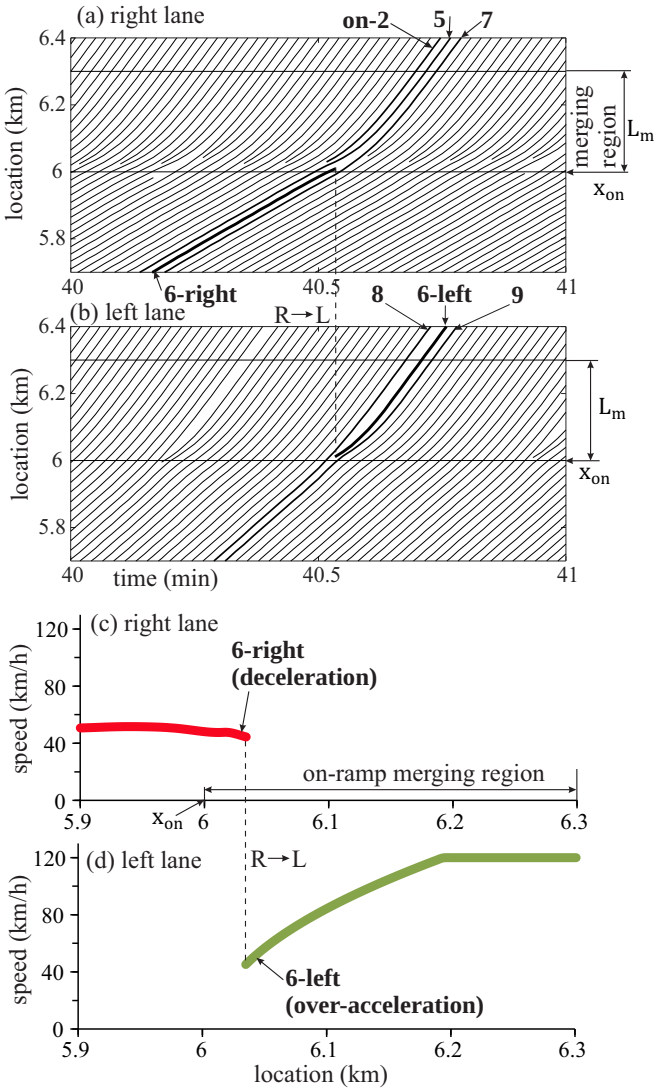


FIG. 6. Continuation of Fig. 4. (a), (b) Simulated vehicle trajectories in synchronized flow at bottleneck in the right lane (a) and left lane (b) at time $t > T_{ind} + \Delta t$. (c), (d) Location-functions of speed of vehicle 6 labeled by "6-right" in the right lane (c) and by "6-left" in left lane (d) in panels (a), (b). R → L lane-changing of vehicle 6 is marked by dashed vertical lines R → L.

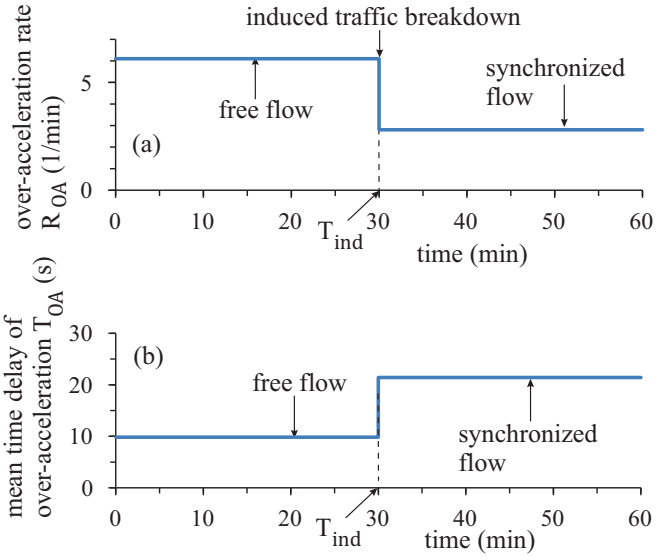


FIG. 7. Continuation of Fig. 4. Induced traffic breakdown (induced F → S transition): (a), (b) Time-dependencies of the over-acceleration rate $R_{OA}$ that is equal to the lane-changing rate $R_{RL}$ (7) (a) and the mean time delay in over-acceleration $T_{OA}$ that is equal to $1/R_{OA}$ (b). Values $R_{OA}$ (a) and $T_{OA}$ (b) have been averaged in free flow (during time interval $0 \leqslant t < 30$ min) and in synchronized flow (during time interval $30 \leqslant t \leqslant 60$ min), respectively.

time headway, safety conditions for lane-changing (6) is more difficult to satisfy in comparison with free flow for which[10] $\tau_{mean}^{(free)} \approx 1.175$ s. The difference in values of $R_{RL}$ in free flow and synchronized flow shown in Fig. 7(a) can already be seen from a comparison of two fragments of vehicle trajectories in the vicinity of the on-ramp merging region shown for free flow in Fig. 5(b)[11] and for synchronized flow in Fig. 6(b).

R → L lane-changing of a vehicle that has initially decelerated in the right lane [for example, vehicle 2-right in Figs. 5(a) and 5(c) and vehicle 6-right in Figs. 6(a) and 6(c) have decelerated before R → L lane-changing] leads to the acceleration of the vehicle in the left lane. Indeed, in free flow, vehicle 2-left in Figs. 5(b) and 5(d) accelerates after R → L lane-changing. In synchronized flow, vehicle 6-left in Figs. 6(b) and 6(d) also accelerates after R → L lane-changing. The vehicle acceleration under consideration is solely determined by R → L lane-changing of the vehicle. Therefore, the rate of the vehicle acceleration denoted by $R_{OA}$, which is caused by R → L lane-changing, is given by formula

$$R_{OA} = R_{RL}. \tag{7}$$

Thus, vehicle acceleration caused by R → L lane-changing exhibits the discontinuous character: In accordance with Eq. (7), there is the discontinuity in the rate of vehicle acceleration $R_{OA}$ when free flow transforms into synchronized flow [Fig. 7(a)].

In next Sec. II D, we explain that the discontinuity in the rate of vehicle acceleration $R_{OA}$ caused by R → L lane-changing leads to the free-flow metastability with respect to the F → S transition (Fig. 4); in three-phase traffic theory, such vehicle acceleration has been called *over-acceleration* [103,106]. Therefore, the acceleration of vehicle 2-left in free flow in Figs. 5(b) and 5(d) as well as the acceleration of vehicle 6-left in synchronized flow [Figs. 6(b) and 6(d)] are examples of over-acceleration; this explains the use of the term *over-acceleration* in Figs. 5–7. We consider also the mean time delay in over-acceleration denoted by $T_{OA}$ that is equal to $1/R_{OA}$; in free flow $T_{OA} \approx 9.84$ s, whereas in

[10]The mean time headway between vehicles in free flow is equal to $\tau_{mean}^{(free)} = (3600/q_{in}) - (d/v_{free}) \approx 1.175$ s.

[11]It should be emphasized that the free-flow state at the bottleneck shown in Fig. 4 during time interval $0 \leqslant t < T_{ind}$ is *identical* with the free-flow state at the bottleneck in Fig. 3. Therefore, parameters of trajectories shown in Fig. 5 are related to both Fig. 3 and to Fig. 4 for time interval $0 \leqslant t < T_{ind}$.

synchronized flow $T_{OA} \approx 21.4$ s [Fig. 7(b)]. The discontinuities in the rate $R_{OA}$ and mean time delay $T_{OA}$ of over-acceleration, i.e., the discontinuous character of over-acceleration found here for automated-driving vehicular traffic is in agreement with three-phase traffic theory for human-driving traffic (Fig. 2).

### D. Spatiotemporal competition of speed adaptation with over-acceleration

There is a spatiotemporal competition between over-acceleration and speed adaptation. In this competition, there are a tendency to free flow and the opposite tendency to synchronized flow. The tendency to free flow is through over-acceleration. The opposite tendency to synchronized flow is through speed adaptation.

Speed adaptation is vehicle deceleration occurring when a vehicle approaches a slower moving preceding vehicle and the following vehicle cannot pass it. We should distinguish speed adaptation in the right lane and speed adaptation in the left lane. This is because speed adaptation in the left lane is caused by a dual role of R → L lane-changing.

#### *1. Tendency to free flow through over-acceleration*

In free flow (Fig. 5) and synchronized flow (Fig. 6), the tendency to free flow through over-acceleration is as follows: A vehicle that changes from the right lane to the left lane permits the following vehicle remaining in the right lane to accelerate. When free flow is currently at the bottleneck, the tendency to free flow through over-acceleration maintains the free-flow state. Indeed, due to over-acceleration of vehicle 2 through its changing to the left lane ["2-left (over-acceleration)" in Fig. 8(a)], the following vehicle 3 remaining in the right lane that trajectory is shown in Fig. 5(a) accelerates [labeled by "3, acceleration" in Fig. 8(a)]. When synchronized flow is currently at the bottleneck, the tendency caused by over-acceleration tries to transform synchronized flow to a free-flow state. For example, due to over-acceleration of vehicle 6 through its changing to the left lane ["6-left (over-acceleration)" in Fig. 8(b)] the following vehicle 7 remaining in the right lane that trajectory is shown in Fig. 6(a) accelerates [labeled by "7, acceleration" in Fig. 8(b)].

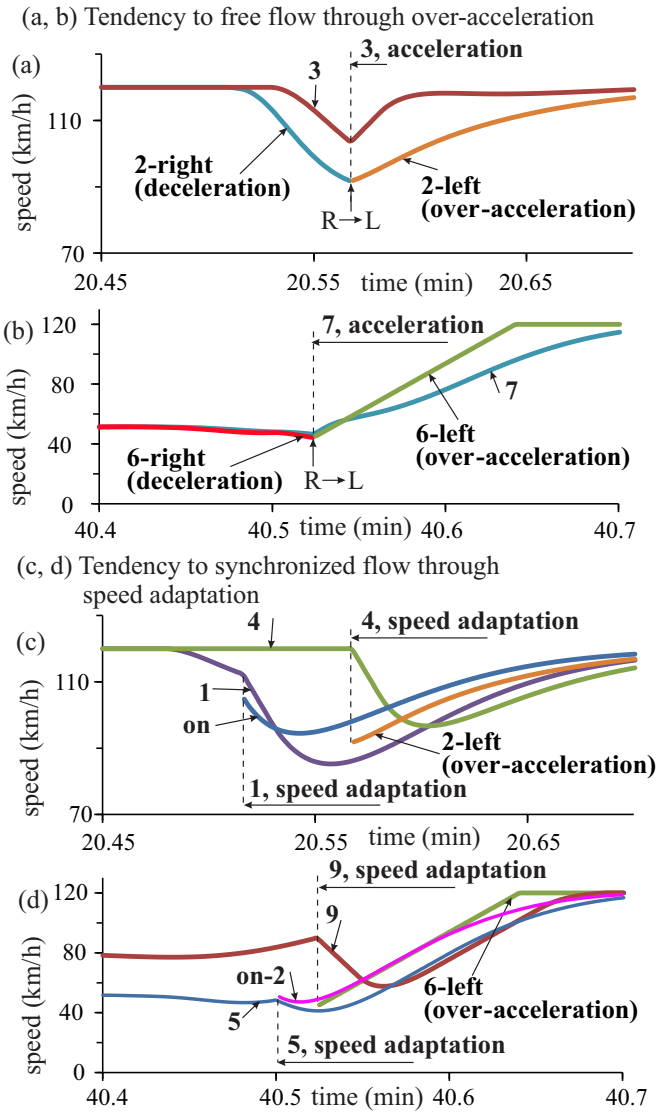


FIG. 8. Simulations of spatiotemporal competition between over-acceleration and speed adaptation. Time-functions of speed for vehicle trajectories presented in Figs. 5(a), 5(b) and 6(a), 6(b) labeled by the same numbers, respectively: (a), (b) Tendency to free flow. (c), (d) Tendency to synchronized flow.

#### *2. Tendency to synchronized flow through speed adaptation in the right lane*

When free flow is at the bottleneck, the tendency caused by speed adaptation tries to transform free flow to synchronized flow [Fig. 8(c)]. A vehicle merging from the on-ramp [vehicle "on" in Figs. 5(a) and 8(c)] forces the following vehicle 1 that trajectory is shown in Fig. 5(a) to decelerate ["1, speed adaptation" in Fig. 8(c)] while adapting the speed to the slower merging vehicle "on."

If synchronized flow is at the bottleneck, the tendency caused by speed adaptation tries to maintain the synchronized flow state [Fig. 8(d)]. A vehicle merging from the on-ramp [vehicle "on-2" in Figs. 6(a) and 8(d)] forces the following vehicle 5 that trajectory is shown in Fig. 6(a) to decelerate [labeled by "5, speed adaptation" in Fig. 8(d)].

#### *3. Tendency to synchronized flow through speed adaptation in the left lane: Dual role of lane-changing*

There is a dual role of lane-changing that is as follows. In free flow, R → L lane-changing of vehicle 2 leads to over-acceleration ["2-left (over-acceleration)" in Figs. 5(a) and 5(d)]. Contrarily, the same lane-changing of vehicle 2 causes speed adaptation in the left lane. Indeed, the following vehicle 4 in the left lane that trajectory is shown in Fig. 5(b) must decelerate ["4, speed adaptation" in Fig. 8(c)], while adapting its speed to the speed of slower vehicle 2 that has just changed from the right lane to the left lane.

Speed adaptation caused by a dual role of lane-changing occurs also in synchronized flow. An example is R → L lane-changing of vehicle 6 ["6-left (over-acceleration)" in Fig. 8(d)]: This vehicle forces the following vehicle 9 in the

left lane that trajectory is shown in Fig. 6(b) to decelerate ["9, speed adaptation" in Fig. 8(d)].

#### *4. Two possible results of competition between over-acceleration and speed adaptation*

In Fig. 5, free flow persists at the bottleneck. This means that at the over-acceleration rate $R_{OA} \approx 6.1\ \text{min}^{-1}$ the tendency to free flow through over-acceleration overcomes the tendency to synchronized flow through speed adaptation. The result of the competition between over-acceleration and speed adaptation is the occurrence of the local speed decrease at the bottleneck without the emergence of synchronized flow [Figs. 3 and 4 (at $t < T_{ind}$)].

Contrarily, in Fig. 6 synchronized flow persists at the bottleneck (labeled by "synchronized flow" in Fig. 4). This means that the tendency to synchronized flow through speed adaptation overcomes the tendency to free flow through over-acceleration. This is because the over-acceleration rate $R_{OA} \approx 2.8\ \text{min}^{-1}$ becomes too small in synchronized flow: Due to the small rate of over-acceleration in synchronized flow the competition between speed adaptation and over-acceleration cannot cause a return transition from synchronized flow to free flow. The competition between speed adaptation and over-acceleration determines the speed in synchronized flow.

Thus, the cause of the free-flow metastability with respect to the F → S transition (Fig. 4) is a spatiotemporal competition between over-acceleration, which exhibits the discontinuous character, and speed adaptation.

### E. Synchronized flow characteristics

#### *1. Synchronization of velocities of upstream fronts of synchronized flow in road lanes*

The speed in synchronized flow in the right lane (vehicle 10 in Fig. 9) is less than the speed in synchronized flow in the left lane (vehicle 11). However, this speed difference does not lead to different velocities of the upstream fronts of synchronized flow in the left and right lanes: These upstream front velocities are synchronized [upstream fronts of synchronized flow are labeled by dashed curves "S-up" in Figs. 9(a) and 9(b)].

The physics of this synchronization effect is associated with R → L lane-changing that occurs in the vicinity of the upstream synchronized flow front in the right lane (Fig. 10). While approaching the upstream front of synchronized flow in the right lane, vehicles decelerate [e.g., vehicle 12 in Figs. 10(a) and 10(c)]. When the upstream front of synchronized flow in the left lane comes even slightly downstream of the upstream front of synchronized flow in the right lane, free flow is realized in the left lane between these upstream synchronized flow fronts; then, between the fronts lane-changing rate $R_{RL}$ increases. This causes R → L lane-changing of a vehicle decelerating to a synchronized flow speed in the vicinity of the upstream front of synchronized flow in the right lane (example of R → L lane-changing for vehicle 13 is marked by dashed vertical lines labeled by R → L in Fig. 10). Due to the lane-changing of a slow moving vehicle 13-right to the left lane (vehicle 13-left), the following vehicle 11 in the left lane begins to decelerate stronger than it has been before

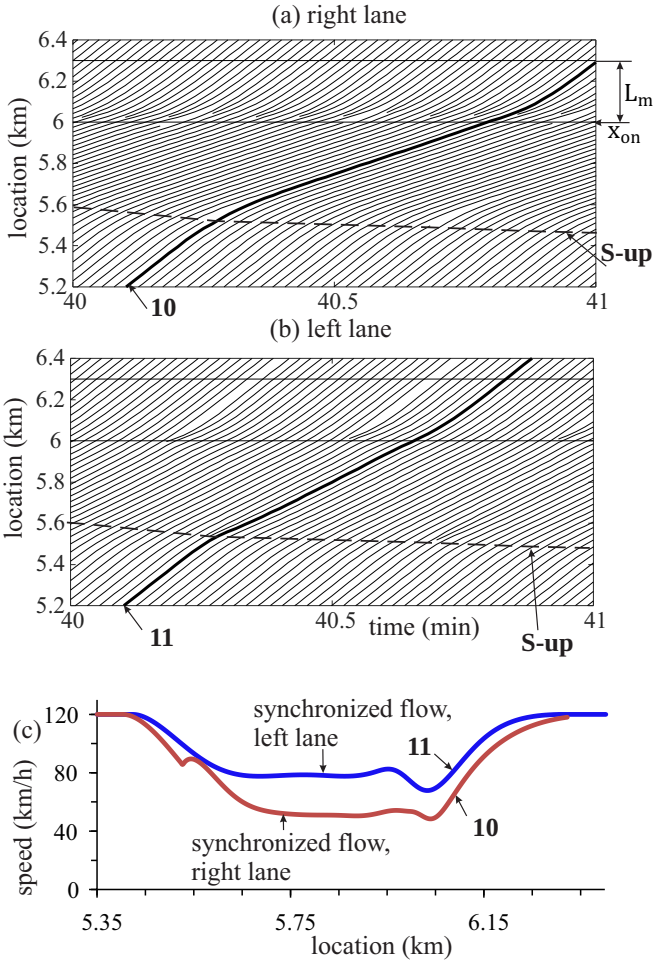


FIG. 9. Continuation of Fig. 6. Features of synchronized flow: (a), (b) Vehicle trajectories at $t > T_{ind} + \Delta t$, i.e., after F → S transition has occurred at the bottleneck. (c), (d) Location-functions of speeds for vehicles 10 and 11 in panels (a), (b).

lane-changing [Fig. 10(d)]. This leads to the synchronization of the upstream front velocities.

#### *2. Effect of discontinuity in lane-changing rate on flow-rate distribution*

In the initial free-flow state existing at the bottleneck at $0 \leqslant t < T_{ind}$ (Fig. 4), R → L lane-changing leads to the nearly fully equalization of the flow rates and densities between the road lanes downstream of the bottleneck (left column in Fig. 11 at $t < T_{ind} = 30$ min). After the F → S transition has occurred, the lane-changing rate in synchronized flow at the bottleneck decreases sharply (discontinuity in the lane-changing rate) and, therefore, the flow rates and densities between lanes cannot be equalized.[12] This explains why in free flow downstream of the bottleneck both the density and

[12]Note that when synchronized flow is at the bottleneck, the flow rate in the left lane depends on both the rate of R → L lane-changing $R_{RL}$ in the vicinity of the downstream front of synchronized flow (Figs. 5–7, Sec. II C) and the rate of R → L lane-changing at the upstream front of synchronized flow (Fig. 10, Sec. II E). For this

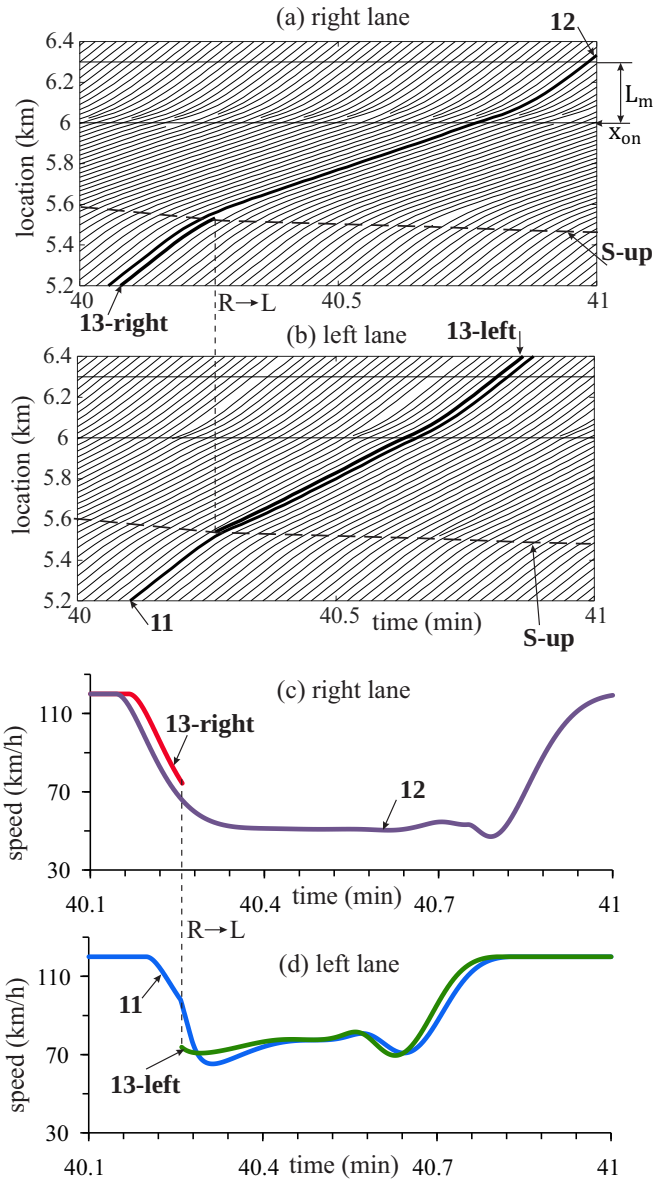


FIG. 10. Continuation of Fig. 9: Synchronization of velocities of upstream fronts of synchronized flow in the right and left lanes. (a), (b) Vehicle trajectories taken from Figs. 9(a) and 9(b). (c), (d) Time-functions of speeds along trajectories marked in panels (a), (b) by the same numbers, respectively.

flow rate are smaller in the left lane than they are, respectively, in the right lane (left column in Fig. 11 at $t \geqslant T_{\rm ind}$).

The discontinuity in the lane-changing rate is also responsible for differences in the averaged speeds, densities, and flow rates in synchronized flow in the right and left lanes upstream of the bottleneck (right column in Fig. 11 at $t \geqslant T_{\rm ind}$).

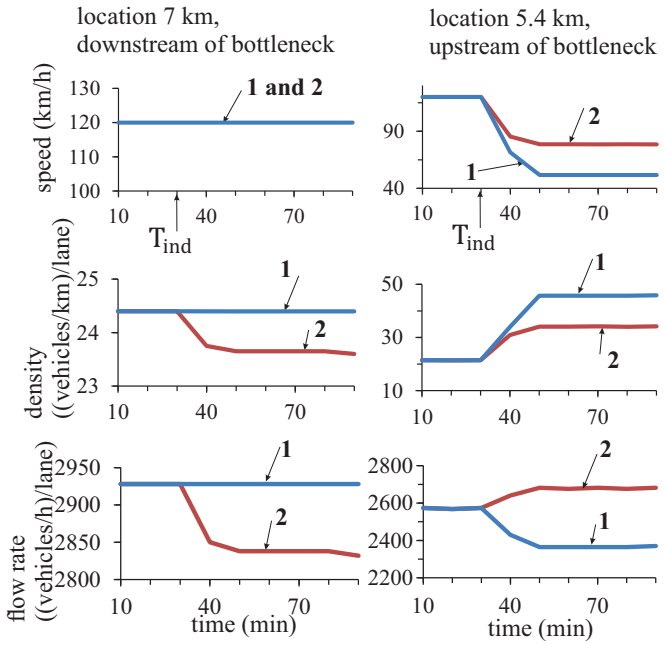


FIG. 11. Continuation of Fig. 4: Time-functions of automated vehicle speed (first line), density (second line), and flow rate (third line) at road location $x = 7$ km [downstream of the bottleneck] (left column) and road location $x = 5.4$ km [upstream of the bottleneck] (right column); curves 1–right lane, curves 2–left lane. 10 min averaging time interval at virtual detectors.

### F. Three-phase traffic theory as a common framework for human-driving and automated-driving traffic

Simulations of automated-driving vehicular traffic [Figs. 12(a) and 12(b)] show the empirical nucleation features of the F → S transition found in measurements of real human-driving traffic [Figs. 1(a) and 1(b)]. Thus, three-phase traffic theory can indeed be considered a common framework for the analysis of the dynamics of human-driving and automated-driving traffic.

A moving synchronized flow pattern (MSP) in Fig. 12(a) has been induced through the use of an on-ramp inflow impulse at a downstream bottleneck (B-down in Fig. 13). While propagating upstream, the MSP induces the F → S transition at the upstream bottleneck.

To simulate a moving bottleneck (MB) in Fig. 12(b), we have assumed that there is a single automated vehicle moving in the right lane at a maximum free-flow speed $v_{\rm MB}$ that is less than $v_{\rm free}$. Already at $v_{\rm MB} = 110$ km/h that is only 10 km/h less than $v_{\rm free}$, the slower vehicle acts as the MB [Figs. 12(b) and 14]. We have also assumed that through the use of cooperative-driving automated vehicles receive the information about the location and speed of the MB. Within a MB merging region of length $L_{\rm M}$, each vehicle moving in the right lane changes to the left lane to pass the MB if safety conditions (6) are satisfied [e.g., see vehicle 1 in Figs. 14(a) and 14(b)]; lane-changing rules (4), (5) are not applied within the MB merging region.[13] Other vehicles for which conditions (6)

reason, the flow-rate difference in the left and right lanes downstream of the bottleneck is less than it would be related to the difference between values $R_{\rm RL} = 6.1$ min$^{-1}$ for free flow and $R_{\rm RL} = 2.8$ min$^{-1}$ for synchronized flow [Fig. 7(a)].

[13]This MB model is the same as that in Ref. [139] used in a stochastic discrete microscopic model for human-driving traffic. In

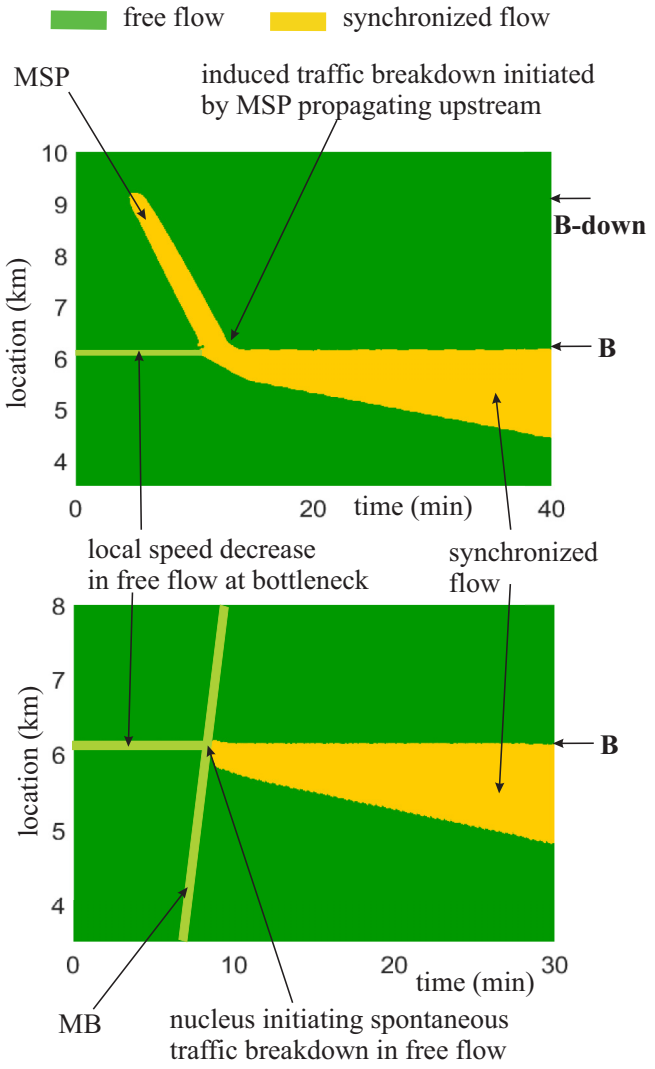


FIG. 12. Simulations of automated-driving vehicular traffic that reproduce empirical breakdown nucleation features measured in real human-driving traffic (Fig. 1). Speed data averaged across two-lane road are presented in space and time in free flow (green) and synchronized flow (yellow): (a) A moving synchronized flow pattern (MSP) induced at the downstream bottleneck (B-down) propagates upstream; reaching the upstream on-ramp bottleneck (B) the MSP induces the F → S transition at the bottleneck. (b) A slow moving vehicle (moving bottleneck—MB) while propagating downstream in free flow acts as a nucleus for empirical spontaneous F → S transition at bottleneck B when the MB propagates through bottleneck B. Both bottleneck B-down and bottleneck B are identical with the on-ramp bottleneck used above (Figs. 3–11); more details of simulations are in Figs. 13 and 14.

are not satisfied have to move at the velocity $v_{MB}$ behind the MB [trajectories of these vehicles are within a region between the MB trajectory and a dashed-dotted line in Fig. 14(a)]. Some vehicles moving in the left lane, after they have passed

accordance with the MB model, lane-changing rules (4), (5) are used only outside the MB merging region.

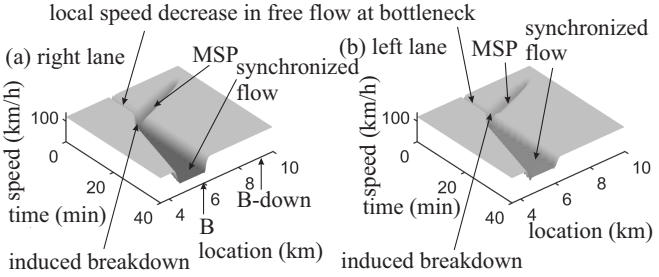


FIG. 13. Simulations of F → S transition through upstream propagation of MSP to upstream bottleneck that in simplified version is shown in Fig. 12(a): Speed in space and time in the right lane (a) and left lane (b). $q_{in} = 2571$ (vehicles/h)/lane. Two-lane road with two bottlenecks: Parameters of upstream bottleneck (B) are $x_{on} = 6$ km, $L_m = 0.3$ km, $q_{on} = 720$ vehicles/h; parameters of downstream bottleneck (B-down) are $x_{on}^{(down)} = 9$ km, $L_m^{(down)} = 0.3$ km, $q_{on}^{(down)} = 0$; road length $L = 10$ km. Parameters of on-ramp inflow impulse at downstream bottleneck B-down applied at $T_{ind}^{(down)} = 5$ min are $\Delta q_{on}^{(down)} = 900$ vehicles/h, $\Delta t^{(down)} = 1$ min. Other model parameters are the same as those in Fig. 3.

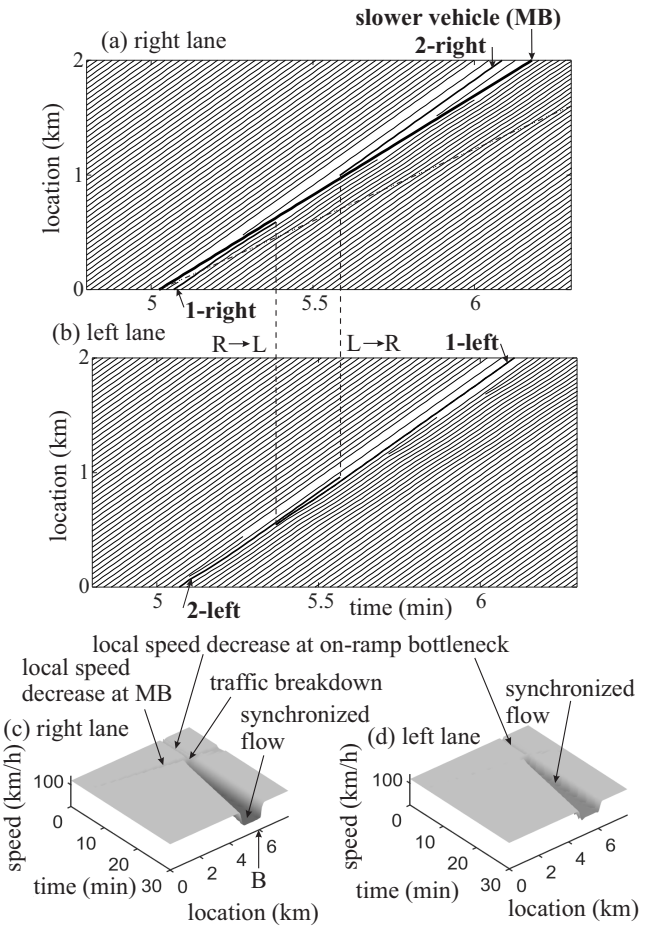


FIG. 14. Simulations of F → S transition occurring due to downstream propagation of MB through the bottleneck that in simplified version is shown in Fig. 12(b): (a), (b) Vehicle trajectories in the vicinity of MB in the right lane (a) and left lane (b). (c), (d) Speed in space and time in the right lane (c) and left lane (d). $q_{in} = 2571$ (vehicles/h)/lane, $q_{on} = 720$ vehicles/h, $L_M = 0.3$ km, $v_{MB} = 110$ km/h. Other model parameters are the same as those in Fig. 3.

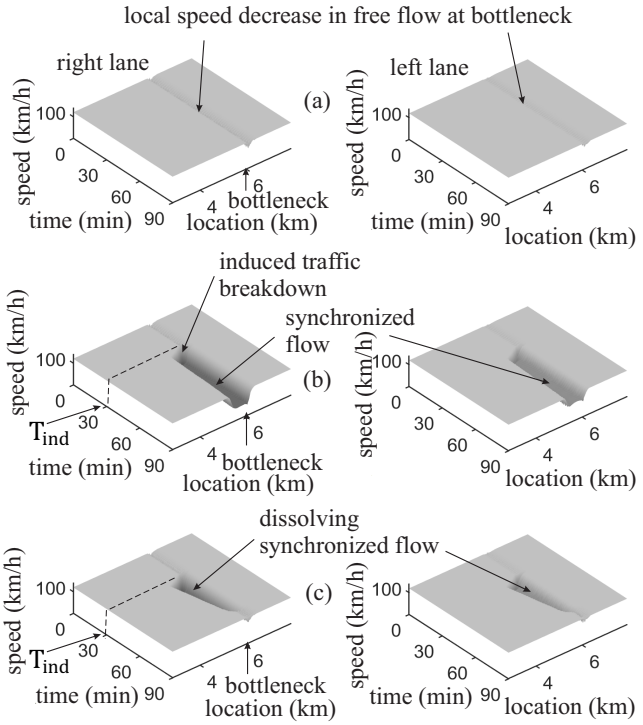


FIG. 15. Simulations of minimum capacity $C_{min} = 2q_{in} + q_{on,min}$ of free flow at bottleneck. Speed in space and time in the right lane (left column) and left lane (right column) at different $q_{on}$ at the same value $q_{in} = 2571$ (vehicles/h)/lane as that in Fig. 3: (a) Free flow. (b) Induced traffic breakdown in panel (a). (c) Induced dissolving synchronized flow. In panels (a), (b), $q_{on} = q_{on,min} = 650$ vehicles/h, i.e., $C_{min} = 5792$ vehicles/h; in panel (c), $q_{on} = 630$ vehicles/h. In panels (b), (c), as explained in Sec. II B, on-ramp inflow rate impulse has been applied; parameters of the impulse inducing either F → S transition (induced traffic breakdown) (b) or dissolving synchronized flow (c) at bottleneck are: $T_{ind} = 30$ min, $\Delta t = 5$ min; $\Delta q_{on} = 250$ vehicles/h in panel (b) and $\Delta q_{on} = 270$ vehicles/h in panel (c). Other model parameters are the same as those in Fig. 3.

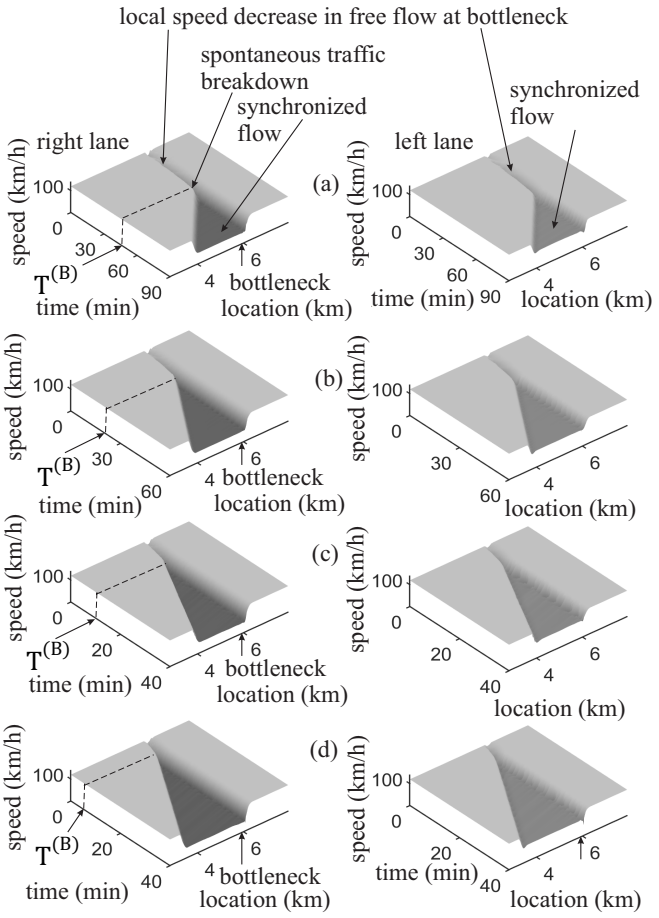


FIG. 16. Simulations of spontaneous F → S transition at bottleneck. Speed in space and time in the right lane (left column) and left lane (right column) at different $q_{on}$ at the same value $q_{in} = 2571$ (vehicles/h)/lane as that in Fig. 3: (a) $q_{on} = 729$ vehicles/h, $T^{(B)} = 51$ min. (b) $q_{on} = 740$ vehicles/h, $T^{(B)} = 19.8$ min. (c) $q_{on} = 760$ vehicles/h, $T^{(B)} = 10$ min. (d) $q_{on} = 780$ vehicles/h, $T^{(B)} = 5$ min. Other model parameters are the same as those in Fig. 3.

the MB location, change back to the right lane where they can move at the speed $v_{free}$ [vehicle 2 in Figs. 14(a) and 14(b)].

The MB causes a speed decrease localized at the MB that moves at the speed $v_{MB}$ [Fig. 14(c)]. As in human-driving traffic [Fig. 1(b)], when the local speed decrease at the MB reaches other local speed decrease at road bottleneck (B), an additional short-time local speed decrease occurs at the bottleneck; this acts as a nucleus for traffic breakdown (F → S transition) at the bottleneck [Figs. 12(b) and 14].

## III. RANGE OF HIGHWAY CAPACITIES AT ANY TIME INSTANT

### A. Minimum and maximum highway capacities

We have found that at any time instant the metastability of free flow in automated-driving vehicular traffic on two-lane road with the bottleneck is realized within a flow rate range

$$C_{min} \leqslant q_{sum} < C_{max}, \tag{8}$$

where $q_{sum} = 2q_{in} + q_{on}$ is the total flow rate across the road in free flow; $C_{min}$ and $C_{max}$ are, respectively, minimum and maximum highway capacities. The physics of the capacity range (8) is that within this capacity range an F → S transition can be induced at the bottleneck. This result is in accordance with the three-phase traffic theory of human-driving traffic.

The minimum capacity $C_{min}$ is explained in Fig. 15: At a given $q_{in}$, there is a minimum on-ramp inflow rate denoted by $q_{on} = q_{on,min}$ at which in an initial free flow at the bottleneck [Fig. 15(a)] an F → S transition can still be induced [Fig. 15(b)]; the minimum capacity is equal to $C_{min} = 2q_{in} + q_{on,min}$. At the model parameters, the F → S transition leads to the formation of a localized synchronized flow pattern (LSP) at the bottleneck [Fig. 15(b)]. Contrarily, if

$$q_{sum} < C_{min}, \tag{9}$$

then no F → S transition can be induced at the bottleneck: Synchronized flow induced at the bottleneck dissolves over time [labeled by "dissolving synchronized flow" in Fig. 15(c)].

When the flow rate $q_{sum}$ increases, a maximum highway capacity $C_{max}$ can be reached. The maximum capacity $C_{max}$ is

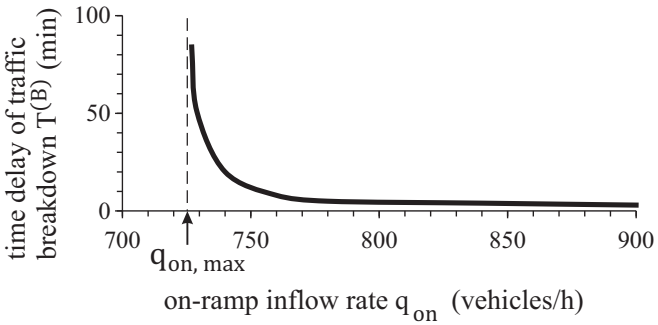


FIG. 17. Continuation of Fig. 16. Dependence of the time delay $T^{(B)}$ of spontaneous F → S transition at bottleneck on the on-ramp inflow rate $q_{on}$ at the given flow rate $q_{in} = 2571$ (vehicles/h)/lane. Calculated values $q_{on,max} = 726$ vehicles/h, $C_{max} = 2q_{in} + q_{on,max} = 5868$ vehicles/h.

a total flow rate $q_{sum}$ that separates two qualitatively different phenomena: (i) When condition (8) is satisfied, then free flow is in a metastable state with respect to the F → S transition at the bottleneck [Figs. 4 and 15(b)]. (ii) When condition

$$q_{sum} > C_{max} \tag{10}$$

is satisfied, then free flow is in an unstable state with respect to a *spontaneous* F → S transition at the bottleneck (Fig. 16). At a given flow rate $q_{in}$, the increase in $q_{sum}$ is achieved through the increase in $q_{on}$. In this case, the maximum capacity $C_{max}$ is reached, when the on-ramp inflow rate $q_{on}$ is equal to some critical value denoted by $q_{on} = q_{on,max}$, i.e., $C_{max} = 2q_{in} + q_{on,max}$.

### B. Time delay of spontaneous traffic breakdown (spontaneous F → S transition)

There is a time delay of the spontaneous F → S transition at the bottleneck denoted by $T^{(B)}$ (Figs. 16 and 17): Under condition (10), it has been found that the less the difference $q_{sum} - C_{max}$, the longer the time delay $T^{(B)}$ is (Fig. 17). In the time-delay–flow-rate plane, condition $q_{sum} = C_{max}$ determines an asymptote (dashed vertical line in Fig. 17) that separates metastable free flow (left of the asymptote) and unstable free flow with respect to the F → S transition (right of the asymptote).[14]

[14]It must be emphasized that we study a *deterministic* model of automated-driving vehicular traffic of Sec. II A, in which *no random* local disturbances of speed, flow rate, or/and density occur. Rather than through random effects, in such a "deterministic limit" of the three-phase traffic theory, local disturbances appear *only* through vehicle interactions with each other. In particular, such vehicle interactions are caused by vehicle merging at the on-ramp bottleneck as well as by the lane-changing behavior. For this reason, if $q_{sum} = C_{max}$, then the traffic system is in a "intermediate" free-flow state in which even a very small additional local speed decrease at the bottleneck causes an F → S transition at the bottleneck. It has been proven that the smaller the additional local speed decrease at the bottleneck is, the longer the time delay $T^{(B)}$ of the F → S transition at the bottleneck.

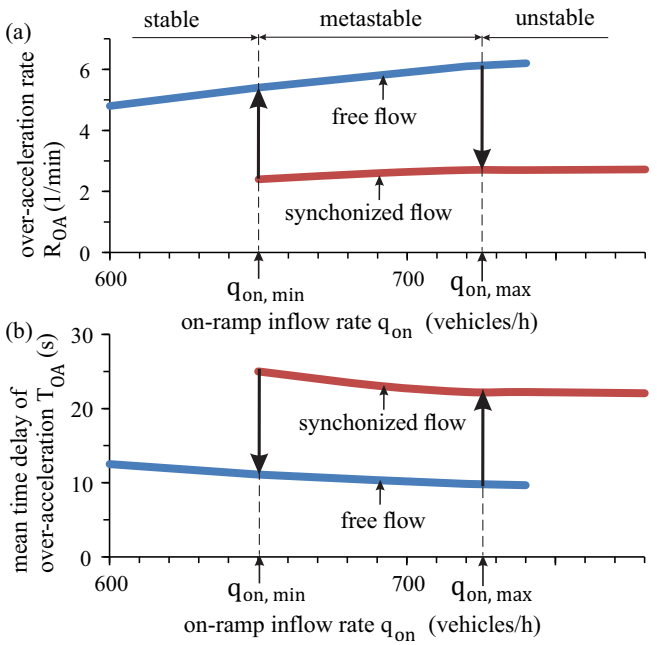


FIG. 18. Simulated range of the discontinuity in over-acceleration rate $R_{OA}$ that is equal to the lane-changing rate $R_{RL}$ (7) (a) and in mean time-delay in over-acceleration $T_{OA}$ that is equal to $1/R_{OA}$ (b) as functions of the on-ramp inflow rate $q_{on}$ at given flow rate $q_{in} = 2571$ (vehicles/h)/lane: Z characteristics of the F → S transition in automated-driving vehicular traffic on two-lane road with bottleneck. Other model parameters are the same as those in Fig. 3.

### C. Range of discontinuity of over-acceleration rate

Within the flow-rate range (8) there can be either a free-flow state or a synchronized flow state at the bottleneck. Under condition $q_{in}$ =const, the range (8) is equivalent to the on-ramp inflow-rate range (Fig. 18)

$$q_{on,min} \leqslant q_{on} < q_{on,max}. \tag{11}$$

When the initial state is free flow and $q_{on}$ increases, then at $q_{on} > q_{on,max}$ a spontaneous F → S transition occurs with a delay time $T^{(B)}$ (Figs. 16 and 17). The emergent synchronized flow persists due to the discontinuity in the over-acceleration rate (Sec. II D): The over-acceleration rate decreases sharply [down-arrow in Fig. 18(a)], respectively, the mean time delay in over-acceleration increases sharply [up-arrow in Fig. 18(b)].

When $q_{on}$ decreases, synchronized flow exists in the range (11). Only when $q_{on}$ becomes less than $q_{on,min}$, a return spontaneous S → F transition occurs at the bottleneck; respectively, free flow recovers at the bottleneck. Thus, there is a Z characteristic for traffic breakdown at the bottleneck that shows stable, metastable, and unstable states of free flow with respect to the F → S transition at the bottleneck (Fig. 18).

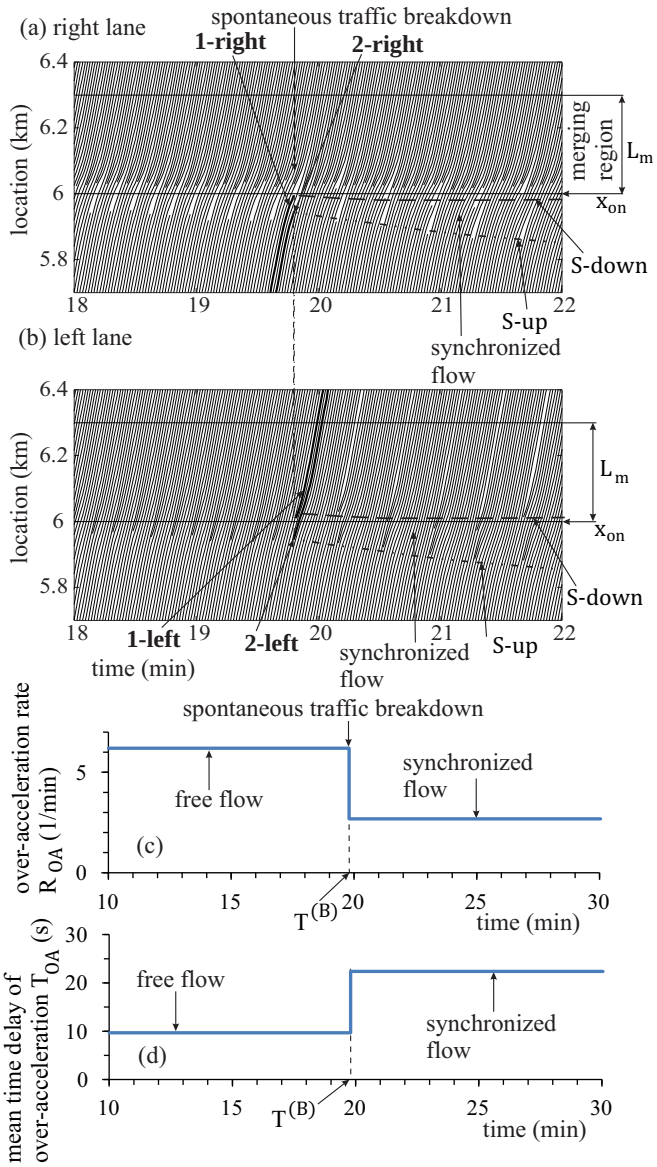


FIG. 19. Continuation of Fig. 16(b). Features of spontaneous traffic breakdown: (a), (b) Vehicle trajectories in the right lane (a) and left lane (b). (c), (d) Time-dependencies of the over-acceleration rate $R_{OA}$ that is equal to the lane-changing rate $R_{RL}$ (7) (c) and the mean time delay in over-acceleration $T_{OA}$ that is equal to $1/R_{OA}$ (d); values $R_{OA}$ (c) and $T_{OA}$ (d) have been averaged in free flow (during time interval 10 min $\leqslant t < T^{(B)}$) and in synchronized flow (during time interval $T^{(B)} \leqslant t \leqslant 30$ min, where $T^{(B)} = 19.8$ min), respectively.

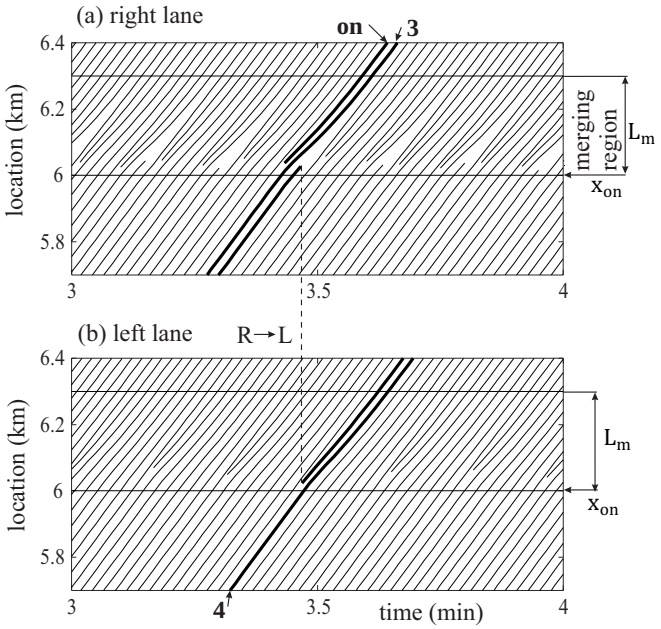


FIG. 20. Continuation of Fig. 16(b): Vehicle trajectories in free flow at the bottleneck at $t \ll T^{(B)}$ in the right lane (a) and left lane (b).

### D. Physics of spontaneous traffic breakdown

The spontaneous F → S transition occurs at $t = T^{(B)}$ (Sec. III B) when a *sequence of two* R → L *lane-changing* occurs: One of them is realized at the downstream front of the local speed decrease [vehicle 1 in Figs. 19(a) and 19(b)] and another occurs at the upstream front of the local speed decrease [vehicle 2 in Figs. 19(a) and 19(b)]. Simultaneously, a drop in the over-acceleration rate $R_{OA}$ [Fig. 19(c)] and, respectively, a jump in the mean time delay in over-acceleration $T_{OA}$ are realized [Fig. 19(d)]. As explained in Sec. II D, this discontinuous behavior of over-acceleration causes the abrupt transformation of the local speed decrease in free flow at the bottleneck into synchronized flow. The boundaries of synchronized flow are given by the downstream synchronized flow front (dashed curves "S-down") fixed at the bottleneck and the upstream synchronized flow front propagating upstream (dashed-dotted curves "S-up" in Figs. 19(a) and 19(b)].

The physics of the maximum capacity $C_{max}$ and time delay $T^{(B)}$ of spontaneous traffic breakdown is as follows. As found, at $q_{on} < q_{on,max}$ the minimum speed within the local speed decrease in free flow at the bottleneck does not almost depend on time (Fig. 3). Contrarily, at $q_{on} > q_{on,max}$ (Fig. 16) the minimum speed within the local speed decrease in free flow grows continuously over time [Figs. 20 and 21(a), 21(b) (at $t < T^{(B)}$)]. Indeed, at $t \ll T^{(B)}$ (Fig. 20) minimum speeds of vehicles 3 and 4 are considerably larger than minimum speeds, respectively, of vehicles 5 and 7 moving in free flow at time that is only about 30 s less than $t = T^{(B)}$ [Figs. 21(c) and 21(d)]. Thus, the maximum capacity $C_{max}$ separates free-flow states at $q_{on} < q_{on,max}$, in which the local speed decrease at the bottleneck does not growth over time, from free-flow states at $q_{on} > q_{on,max}$, in which the local speed decrease does continuously grow over time.[15]

The continuous reduction of the minimum speed within the local speed decrease in free flow at the bottleneck over time has to have a limit that can be considered a critical minimum speed: After vehicle "on-3" has merged from the on-ramp, minimum speeds of vehicles 8 and 9 moving in the right

[15]Note that during the growth of the local speed decrease in free flow at the bottleneck, locations of R → L lane-changing move slowly upstream while remaining in the vicinity of location $x = x_{on}$ [compare locations of R → L lane-changing in Fig. 20(b) with locations of R → L lane-changing in Fig. 21(b) (at $t < T^{(B)}$)].

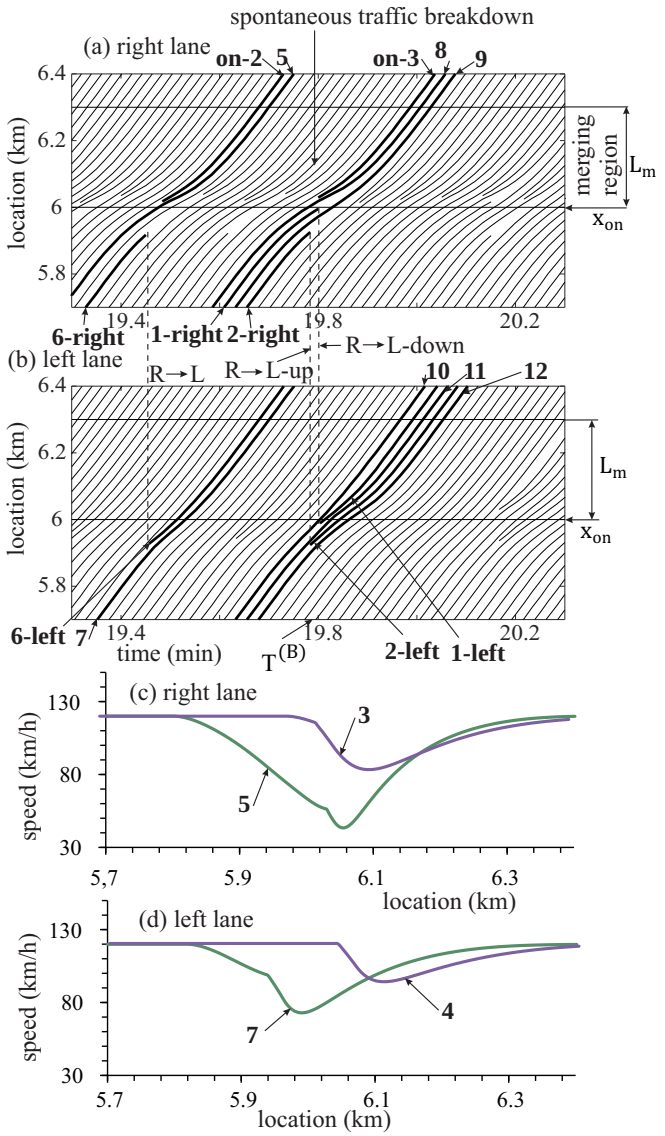


FIG. 21. Continuation of Fig. 16(b). (a), (b) Vehicle trajectories in the right lane (a) and left lane (b); trajectories "on-2," 5–7 are in free flow at time that is about 30 s less than $t = T^{(B)}$; trajectories "on-3," 8–12 are related to the time of traffic breakdown (F → S transition) $t = T^{(B)}$. (c), (d) Comparison of location-functions of speeds for vehicles 3 and 4 taken from Fig. 20 with speeds on trajectories 5 and 7 from (a), (b). Vehicles 1 and 2 are, respectively, the same as that in Figs. 19(a) and 19(b). Sequence of two R → L lane-changing effects of vehicles 1 and 2 that causes spontaneous traffic breakdown are labeled by R → L-down and R → L-up, respectively.

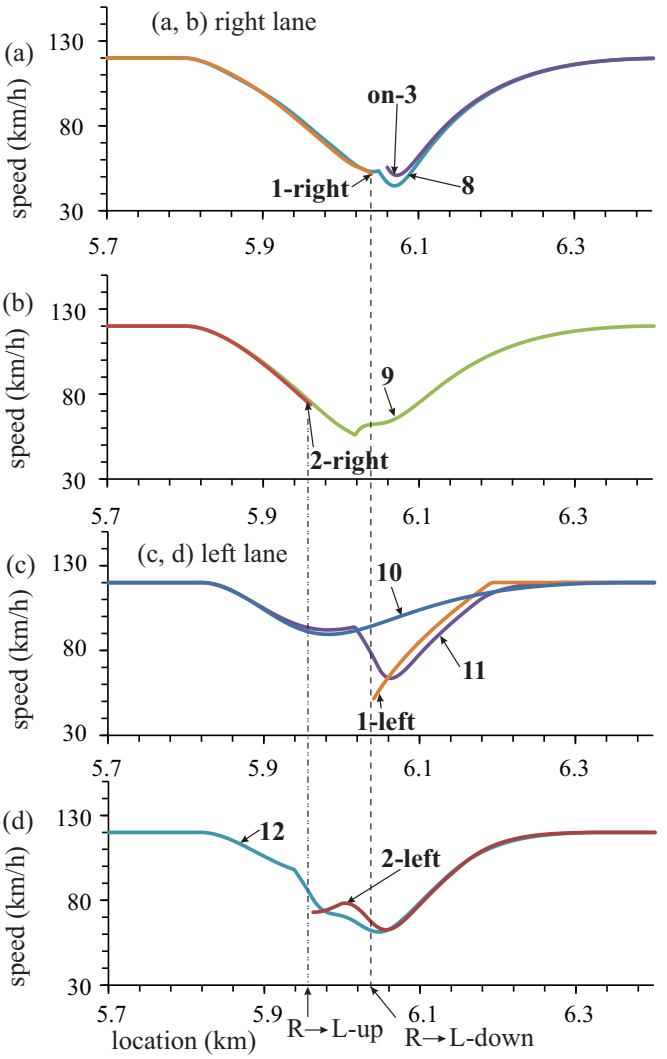


FIG. 22. Continuation of Fig. 21: Location-functions of speed for some vehicles whose numbers are the same as that in Fig. 21, respectively; vehicles 1 and 2 are, respectively, the same as that in Figs. 19(a) and 19(b).

lane become low enough [Figs. 21(a) and 22(a), 22(b)]. This causes the sequence of two R → L lane-changing of vehicles 1 and 2 [Figs. 21(a), 21(b) and 22(a), 22(b)]. Slow vehicles 1-left and 2-left [Figs. 22(c) and 22(d)] force, respectively, the following vehicles 11 and 12 moving in the left lane to decelerate strongly. At so low speed in the left lane the over-acceleration rate $R_{OA}$ drops and, respectively, the mean time delay in over-acceleration increases sharply [Figs. 19(c) and 19(d)]; as a result, the speed adaptation overcomes the over-acceleration.

It takes some time for the continuous reduction of the minimum speed within the local speed decrease to the critical speed in free flow at which traffic breakdown occurs at the bottleneck. This time interval determines time delay $T^{(B)}$ of traffic breakdown (F → S transition). We have found that the more the on-ramp inflow rate $q_{on}$ exceeds the critical value $q_{on,max}$, the quicker the critical minimum speed in free flow at the bottleneck is reached. This explains the decreasing character of function $T^{(B)}(q_{on})$ (Fig. 17).

## IV. GENERALIZATION OF NUCLEATION FEATURES OF F → S TRANSITION IN AUTOMATED-DRIVING TRAFFIC

Up to now we have used only one chosen set of model parameters, to demonstrate that automated-driving vehicular traffic does exhibit the basic feature of the three-phase traffic theory—the nucleation character of an F → S transition (traffic breakdown) at the bottleneck. To disclose the physics of this F → S transition, we have studied its features under

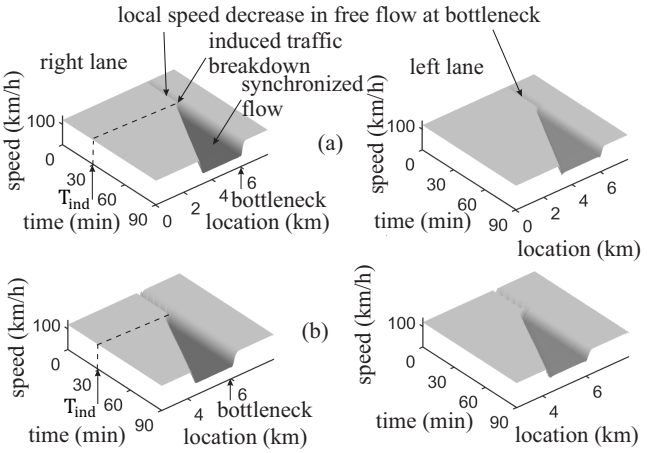


FIG. 23. Speed in space and time in the right lane (left column) and left lane (right column) at the same flow rate $q_{in} = 2571$ (vehicles/h)/lane as that in Fig. 3. (a), (b) Induced F → S transition that has been simulated as that in Fig. 4. (a) Symmetric lane-changing parameters $\delta_1 = \delta_2 = 1$ m/s in Eqs. (4), (5), $q_{on} = 720$ vehicles/h, $\Delta q_{on} = 180$ vehicles/h. (b) Symmetric safety parameters $\tau_1 = \tau_2 = 0.4$ s in Eq. (6), $q_{on} = 700$ vehicles/h, $\Delta q_{on} = 200$ vehicles/h. $T_{ind} = 30$ min, $\Delta t = 2$ min. Other model parameters are the same as those in Fig. 3.

a change in the on-ramp inflow rate $q_{on}$ at the bottleneck (Secs. II and III). However, do basic results of this paper about the nucleation character of the F → S transition at the bottleneck and the existence of a range of highway capacities remain in automated-driving vehicular traffic, when model parameters are changed?

### A. Effect of lane-changing model parameters on F → S transition

We have found that as long as model parameters in lane-changing rules (4)–(6) enable a distribution of on-ramp inflow between road lanes in free flow, all qualitative results presented above remain the same ones. Examples are shown in Fig. 23 for symmetric lane-changing parameters $\delta_1 = \delta_2$ in Eqs. (4), (5) [Fig. 23(a)] and for symmetric safety parameters $\tau_1 = \tau_2$ in Eq. (6).

### B. Diagrams of F → S transition at bottleneck

To understand the nucleation nature of the F → S transition in automated-driving traffic, up to now we have used only one given flow rate in free flow upstream of the bottleneck $q_{in} = 2571$ (vehicles/h)/lane. We have found that the nucleation nature of the F → S transition at the bottleneck remains when $q_{in}$ changes (Fig. 24). In particular, maximum capacity $C_{max}$ does not almost depend on $q_{on}$, whereas minimum capacity $C_{min}$ is a decreasing function of $q_{on}$: the larger the on-ramp inflow rate $q_{on}$, the larger the capacity range $C_{max} - C_{min}$ [Fig. 24(c)]. When the flow rate $q_{on}$ increases, the flow-rate range $q_{on,max} - q_{on,min}$, within which free flow is metastable with respect to the F → S transition at the bottleneck, increases [Fig. 24(d)].

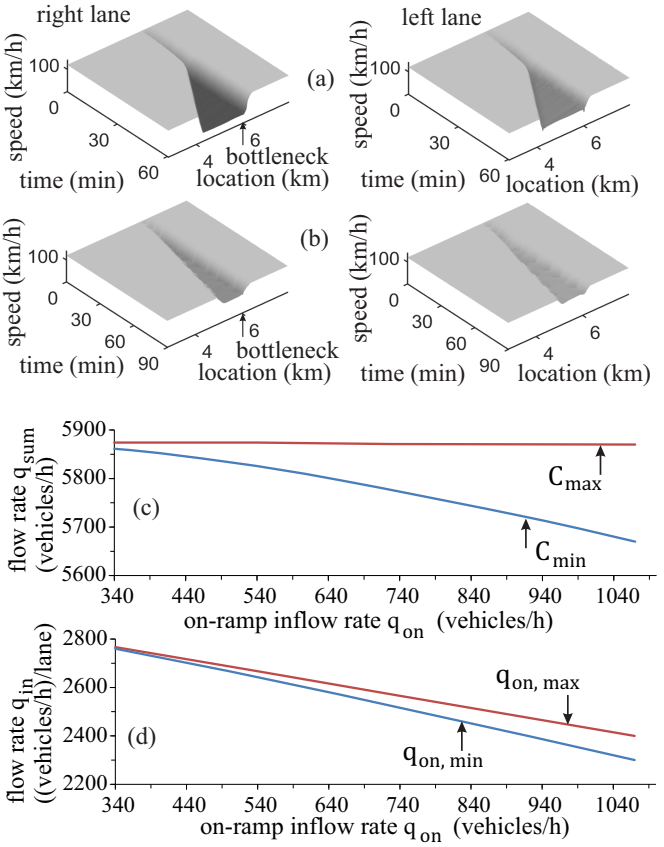


FIG. 24. Simulations of the nucleation nature of the F → S transition at the bottleneck for different values $q_{in}$: (a), (b) Speed in space and time in the right lane (left column) and left lane (right column) for spontaneous F → S transition: (a) $q_{in} = 2449$ (vehicles/h)/lane, $q_{on} = 980$ vehicles/h, $T^{(B)} = 26$ min. (b) $q_{in} = 2769$ (vehicles/h)/lane, $q_{on} = 340$ vehicles/h, $T^{(B)} = 24$ min. (c) Dependencies of minimum highway capacity $C_{min}$ and maximum highway capacity $C_{max}$ on $q_{on}$. (d) Dependencies $q_{in}(q_{on})$ related to $C_{min}(q_{on})$ (curve denoted by $q_{on,min}$) and to $C_{max}(q_{on})$ (curve denoted by $q_{on,max}$), respectively. Other model parameters are the same as those in Fig. 3.

At any value $q_{in}$, at which the F → S transition can occur, the physics of the F → S transition is qualitatively the same as that disclosed in Secs. II and III. In particular, the nature of the F → S transition is caused by the discontinuous character of over-acceleration [Figs. 25(a) and 25(b)] as well as its competition with speed adaptation. Features of synchronized flow occurring due to the F → S transition (Sec. II E) remain also the same when $q_{in}$ changes. The speeds in synchronized flow in the right and left lanes at the bottleneck are decreasing functions of the on-ramp inflow rate [Fig. 25(c)].

### C. Lane-asymmetric nucleation of F → S transition

Because the nucleation nature of F → S transition in automated-driving traffic at the bottleneck is determined by the existence of the discontinuity in R → L lane-changing rate (Sec. II), a question can arise: Does the nucleation nature

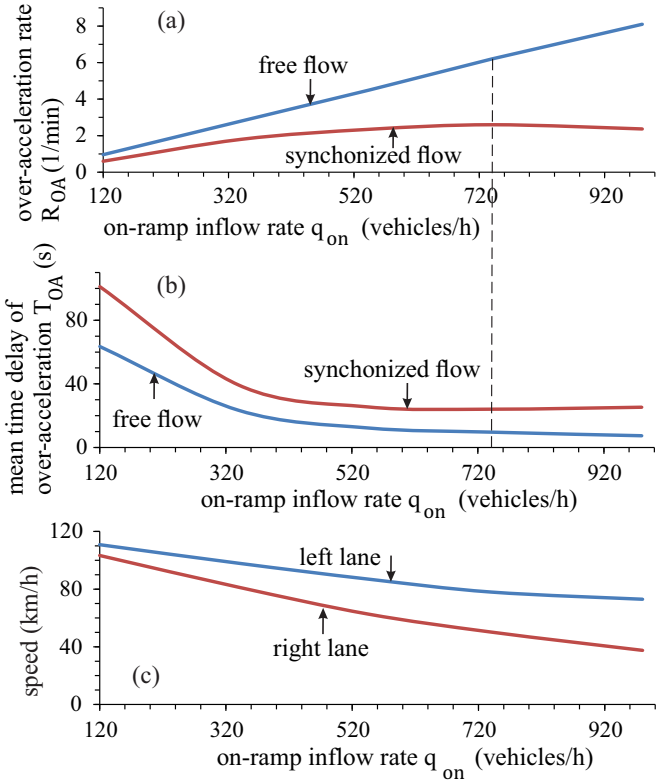


FIG. 25. Characteristics of spontaneous F → S transition at different flow rates $q_{in}$ in free flow upstream of bottleneck. (a), (b) The discontinuous character of over-acceleration: On-ramp inflow-rate dependencies of the over-acceleration rate $R_{OA}$ that is equal to the lane-changing rate $R_{RL}$ (7) (a) and the mean time delay in over-acceleration $T_{OA}$ that is equal to $1/R_{OA}$ (b) in initial free flow (curves "free flow") and in synchronized flow (curves "synchronized flow") that has occurred due to F → S transition. (c) Synchronized flow speeds occurring at the bottleneck after the F → S transition in the right and left lanes. In panels (a), (b), on-ramp inflow-rates $q_{on}$ at the x-axis slightly exceed corresponding values $q_{on,max}$ (we have used $q_{on} = q_{on,max} + \delta q$, where parameter $\delta q = 14$ vehicles/h) calculated by different values $q_{in}$; for explanations of panels (a), (b), a dashed vertical line related to $q_{on} = 740$ vehicles/h has been drawn to show, respectively, the same values $R_{OA}$ and $T_{OA}$ at curves $R_{OA}(q_{on})$ and $T_{OA}(q_{on})$ as those in Figs. 19(c) and 19(d) for $q_{in} = 2571$ (vehicles/h)/lane. Other model parameters are the same as those in Fig. 3.

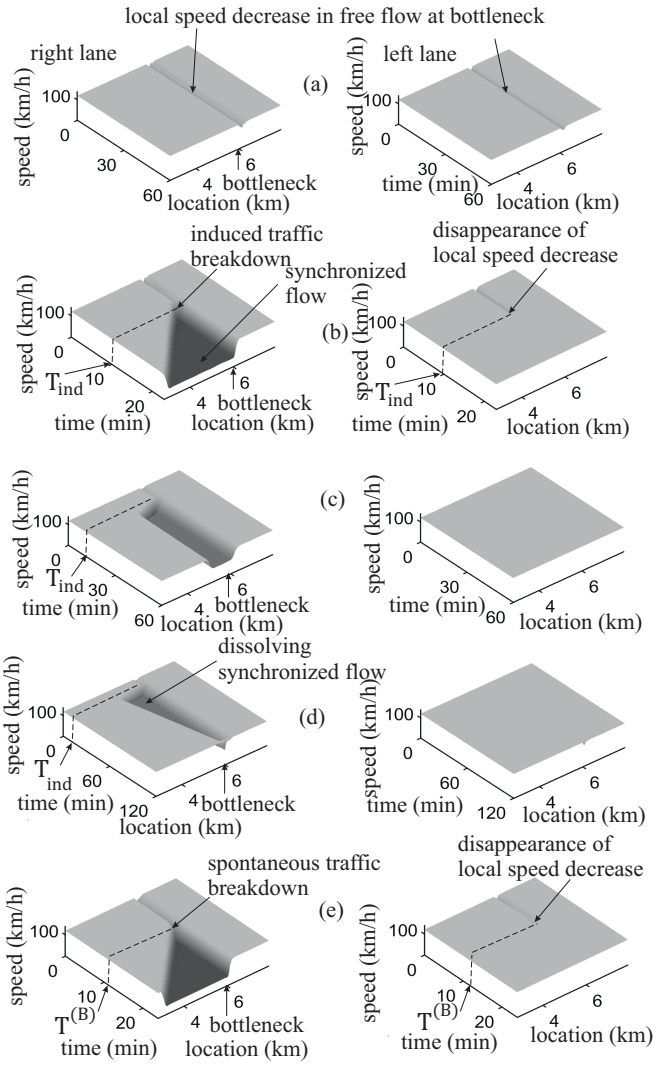


FIG. 26. Simulations of lane-asymmetric F → S transition at bottleneck that occurs in model of Sec. II A, when, in addition to safety conditions (6), condition (12) is used. Speed in space and time in the right lane (left column) and left lane (right column) at different $q_{on}$ at the same flow rate $q_{in} = 2571$ (vehicles/h)/lane as that in Fig. 3: (a) Local speed decrease at bottleneck in free flow, $q_{on} = 720$ vehicles/h. (b) Induced F → S transition in free flow of (a); parameters of on-ramp inflow impulse: $T_{ind} = 10$ min, $\Delta q_{on} = 180$ vehicles/h, $\Delta t = 1$ min. (c) Induced F → S transition at $q_{on} = q_{on,min} = 360$ vehicles/h; $T_{ind} = 10$ min, $\Delta q_{on} = 540$ vehicles/h, $\Delta t = 2$ min. (d) Dissolving synchronized flow at $q_{on} = 350$ vehicles/h that is less than $q_{on,min}$; $T_{ind} = 10$ min, $\Delta q_{on} = 550$ vehicles/h, $\Delta t = 2$ min. (e) Spontaneous F → S transition at $q_{on} = 727$ vehicles/h that is larger than $q_{on,max} = 724$ vehicles/h; $T^{(B)} = 11.5$ min. In Eq. (12), $T_p = 3.3$ s, $g_p = 2$ m. Other model parameters are the same as those in Fig. 3.

of F → S transition remain if the lane-changing rules are changed qualitatively? Indeed, as known, cooperative driving in automated-driving traffic could permit the realization of different lane-changing rules that enable a distribution of on-ramp inflow between road lanes in free flow as done through lane-changing rules (4)–(6). In Eqs. (4)–(6), at a large speed difference between lanes no speed limitation for lane-changing has been assumed. When a vehicle moving at a slow speed $v(t)$ changes from the right lane to the left lane, the vehicle can force the following vehicle moving at a larger speed $v^-(t)$ to decelerate strongly. This can considerably decrease comfortable driving and sometimes traffic safety.

Cooperative driving can solve this problem through some safety condition

$$g^-(t) + [v(t) - v^-(t)]T_p > g_p \tag{12}$$

used in addition to Eq. (6). Safety condition (12), in which $T_p$ and $g_p$ are constant parameters, limits R → L lane-changing, when speed difference $v^-(t) - v(t)$ is large enough, whereas

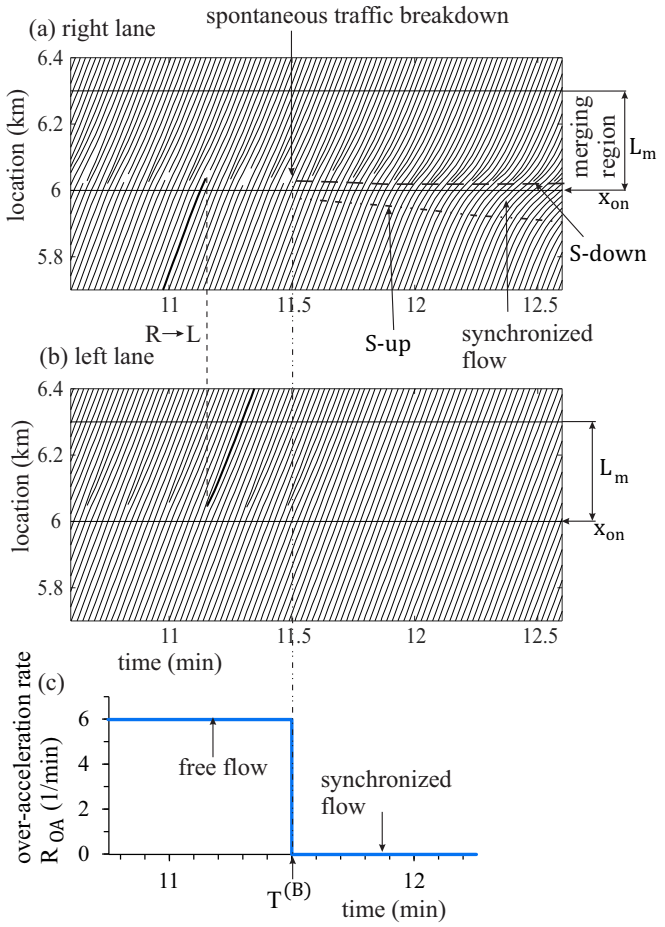


FIG. 27. Continuation of Fig. 26(e). Features of lane-asymmetric spontaneous traffic breakdown: (a), (b) Vehicle trajectories in the right lane (a) and left lane (b). (c) Time-dependence of the over-acceleration rate $R_{OA}$ that is equal to the lane-changing rate $R_{RL}$ (7); value $R_{OA}$ in free flow has been averaged during time interval $0 \leqslant t < T^{(B)}$, where $T^{(B)} = 11.5$ min.

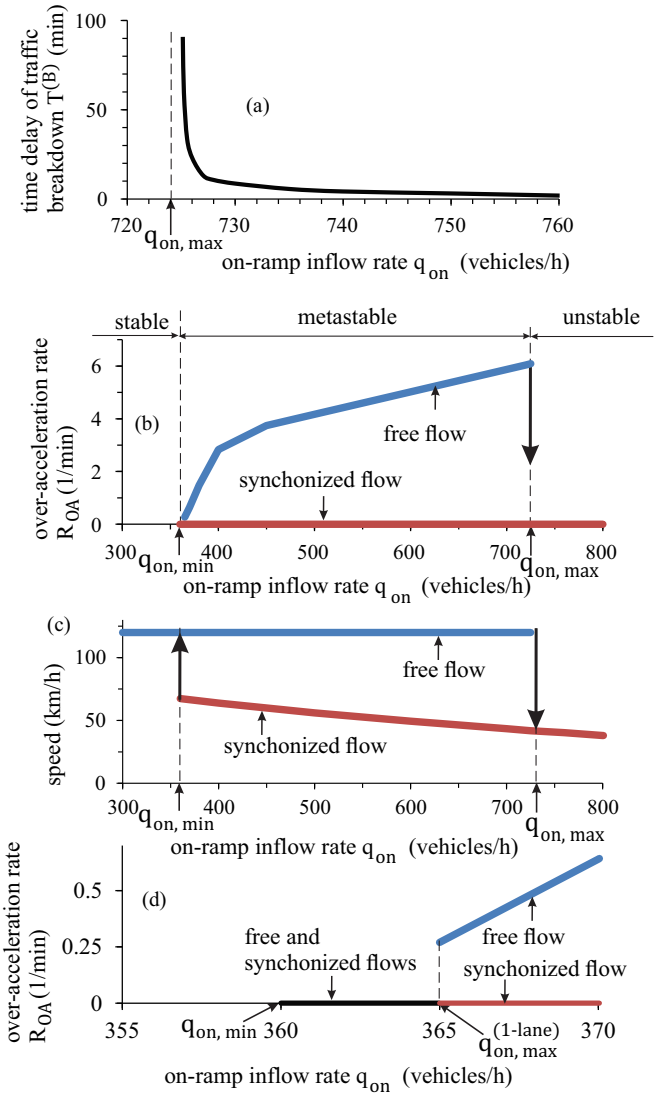


FIG. 28. Simulated characteristics of lane-asymmetric F → S transition on two-lane road with bottleneck at the same value $q_{in} = 2571$ (vehicles/h)/lane as that in Figs. 3–11. (a) Dependence of time delay $T^{(B)}$ of spontaneous traffic breakdown on $q_{on}$; $q_{on,max} = 724$ vehicles/h, $C_{max} = 2q_{in} + q_{on,max} = 5868$ vehicles/h. (b), (c) Simulated Z characteristics of the lane-asymmetric F → S transition: The discontinuity in over-acceleration rate $R_{OA}$ that is equal to the lane-changing rate $R_{RL}$ (7) (b) and speed (c) as functions of $q_{on}$; $q_{on,min} = 360$ vehicles/h, $C_{min} = 2q_{in} + q_{on,min} = 5502$ vehicles/h. (d) A small part of panel (b) in a large scale in vicinity of $q_{on} = q_{on,min}$; $q_{on,max}^{(1-lane)} = 365.2$ vehicles/h. Other model parameters are the same as those in Fig. 26.

the space gap $g^-(t)$ between these vehicles is not large enough for comfortable driving.[16]

### *1. Characteristics of lane-asymmetric nucleation of* F → S *transition*

Condition (12) does not affect on R → L lane-changing in *free* flow [Fig. 26(a)]: The same lane-changing rate is realized and the same local speed decrease appears at the bottleneck as that in Fig. 3. There is free-flow metastability with respect to the F → S transition at the bottleneck as found in Secs. II and III; condition (8) is also valid. Moreover, values $q_{on,max}$ and, respectively, $C_{max} = 2q_{in} + q_{on,max}$, which separate metastable free flow from unstable free flow with respect to the F → S transition at the bottleneck, remain almost the same (Figs. 26–28).

However, the use of condition (12) changes basically the result of the F → S transition at the bottleneck: In Sec. II, after the F → S transition has occurred, synchronized flow emerges both in the right and left lanes (Figs. 4 and 16). Contrarily, under condition (12) the F → S transition causes synchro-

[16]To show the effect of the limitation of the speed difference during R → L lane-changing on phase transitions in automated-driving vehicular traffic, we have used a simple formulation (12). A study of more detailed dynamic models of lane-changing that incorporate reactions on lane-changing of the following vehicles moving in the left lane is out of the scope of this paper; this could be a very interesting task for further traffic studies.

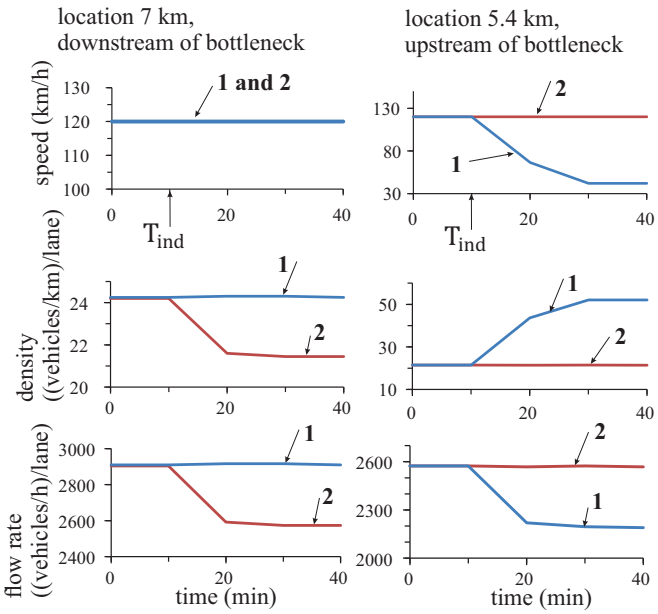


FIG. 29. Continuation of Fig. 26(b): Time-functions of automated vehicle speed (first line), density (second line), and flow rate (third line) at road location $x = 7$ km [downstream of the bottleneck] (left column) and road location $x = 5.4$ km [upstream of the bottleneck] (right column); curves 1—right lane, curves 2—left lane. 10 min averaging time interval at virtual detectors.

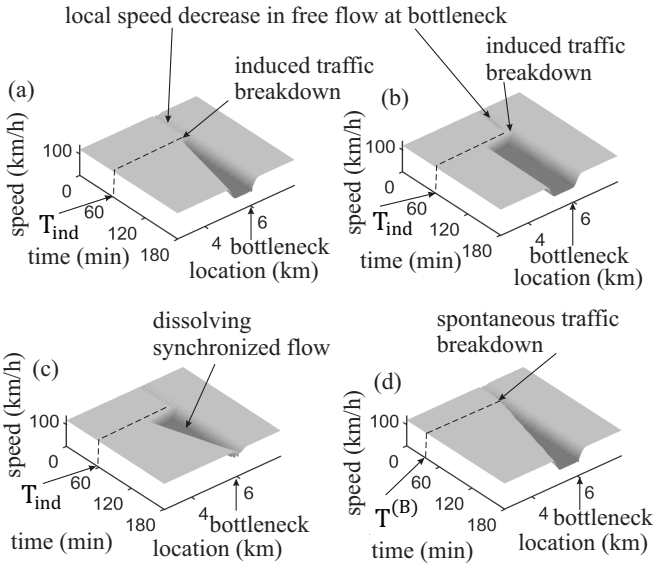


FIG. 30. Simulations of F → S transition on single-lane road with bottleneck model of Sec. II A. Speed in space and time at different $q_{on}$ at the same value $q_{in} = 2571$ vehicles/h as that in Fig. 3: (a) Induced traffic breakdown in metastable free flow at $q_{on} = 365$ vehicles/h, $T_{ind} = 60$ min, $\Delta q_{on} = 135$ vehicles/h, $\Delta t = 1$ min; (b) Induced traffic breakdown in metastable free flow at $q_{on} = 360$ vehicles/h, $T_{ind} = 60$ min, $\Delta q_{on} = 540$ vehicles/h, $\Delta t = 2$ min; (c) Dissolving synchronized flow at $q_{on} = 350$ vehicles/h, $T_{ind} = 60$ min, $\Delta q_{on} = 550$ vehicles/h, $\Delta t = 2$ min; (d) Time-delayed spontaneous traffic breakdown at $q_{on} = 366$ vehicles/h, $T^{(B)} = 30$ min. Other model parameters are the same as those in Fig. 3.

nized flow emergence in the right lane *only* [Figs. 26(b)–26(e)]. For this reason, we can call the F → S transition as a *lane-asymmetric* F → S transition at the bottleneck.

Moreover, after the lane-asymmetric F → S transition has occurred *no* local speed decrease remains in free flow in the left lane at the bottleneck [right column in Figs. 26(b)–26(e)]. The disappearance of the local speed decrease in free flow in the left lane at the bottleneck is explained by the drop in the R → L lane-changing rate to zero during the lane-asymmetric F → S transition (Fig. 27): No R → L lane-changing is realized at $t > T^{(B)}$, i.e., after the lane-asymmetric F → S transition has occurred at $t = T^{(B)}$ [Figs. 27(a) and 27(b)]. Respectively, there is a drop in the over-acceleration rate $R_{OA}$ from the rate $R_{OA}$ in free flow to $R_{OA} = 0$ in synchronized flow [Fig. 27(c); one of these R → L lane-changing in free flow at $t < T^{(B)}$ is marked by dashed vertical line R → L in Figs. 27(a) and 27(b)].[17] The physics of this effect is as follows. When synchronized flow begins to emerge in the right lane, the speed difference $v^{-}(t) - v(t)$ in Eq. (12) becomes large enough. This prevents the R → L lane-changing.

We have found that as in Fig. 17, time delay $T^{(B)}$ of spontaneous lane-asymmetric F → S transition that occurs at $q_{on} > q_{on,max}$ is also a strongly falling on-ramp inflow-rate function [Fig. 28(a)]. However, under the lane-asymmetric F → S transition there is a considerable reduction in values $q_{on,min}$ and, respectively, $C_{min} = 2q_{in} + q_{on,min}$ [Figs. 28(b) and 28(c)] in comparison with these values found in Sec. III (Fig. 15). Other peculiarities of the lane-asymmetric F → S transition have been found when $q_{on}$ decreases: (i) The value $R_{OA}$ decreases strongly [Fig. 28(b)]. (ii) The discontinuity in the over-acceleration rate $R_{OA}$ remains until some inflow-rate denoted by $q_{on,max}^{(1-lane)}$ that slightly exceeds $q_{on,min}$ [Fig. 28(d)]. (iii) Although within the range $q_{on,min} \leqslant q_{on} < q_{on,max}^{(1-lane)}$ free flow is still metastable with respect to the lane-asymmetric F → S transition, nevertheless, the discontinuity in the over-acceleration rate $R_{OA}$ does not exist any more: there is no lane-changing within the inflow-rate range $q_{on,min} \leqslant q_{on} < q_{on,max}^{(1-lane)}$ at all. To understand this result, we consider in Sec. IV C 2 automated-driving traffic on a single-lane road with the same bottleneck.

As in Fig. 11, in the initial free-flow state existing at the bottleneck at $0 \leqslant t < T_{ind}$ [Fig. 26(b)], R → L lane-changing leads to the nearly fully equalization of the flow rates and densities between the road lanes downstream of the bottleneck (left column in Fig. 29 at $t < T_{ind} = 10$ min). After the lane-asymmetric F → S transition has occurred, the rate of R → L lane-changing $R_{RL} = 0$, i.e., there is no R → L lane-changing at all. For this reason, contrary to the case shown in Fig. 11 at $t \geqslant T_{ind} = 30$ min (when synchronized flow is at the bottleneck), in the case of the lane-asymmetric F→ transition under consideration the flow-rate difference in the left and right lanes downstream of the bottleneck is fully

[17] The rate $R_{OA}$ in free flow is nearly the same as that when condition (12) is not used (Secs. II–IV B).

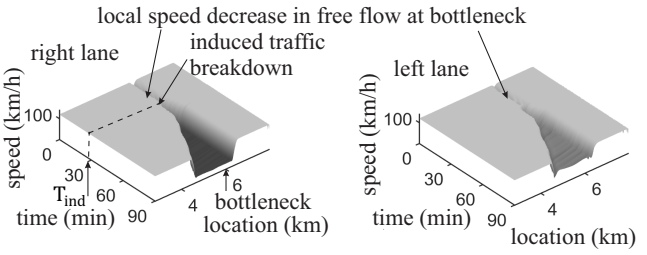


FIG. 31. Simulations of the effect of the increase in desired time headway $\tau_d$ of automated vehicles on nucleation features of F → S transition with the model of Sec. II A on two-lane road with bottleneck: Speed in space and time in the right lane (left) and left lane (right). Induced traffic breakdown under condition (8). $\tau_d = 1.5$ s, $K_1 = 0.3\ \text{s}^{-2}$, $K_2 = 0.6\ \text{s}^{-1}$ in Eqs. (1), (2), $\tau_1 = \tau_2 = 0.9$ s in Eq. (6), $q_{in} = 1714$ (vehicles/h)/lane, $q_{on} = 710$ vehicles/h, $T_{ind} = 30$ min, $\Delta q_{on} = 190$ vehicles/h, $\Delta t = 2$ min. Other model parameters are the same as those in Fig. 3.

determined by the difference between values $R_{RL} \approx 6\ \text{min}^{-1}$ for free flow and $R_{RL} = 0$ for synchronized flow: Downstream of the bottleneck (left column in Fig. 29 at $t > T_{ind}$) the flow rate in the left lane reduces over time to the value $q_{in}$. Because after the lane-asymmetric F → S transition has occurred the rate $R_{RL} = 0$, the averaged speed, density, and flow rate in the left lane upstream of the bottleneck (right column in Fig. 29) do not depend on time.

#### *2. Over-acceleration in automated-driving traffic on single-lane road*

As emphasized above, after the lane-asymmetric F → S transition has occurred, *no* effect of the bottleneck on the vehicle motion in the left lane is realized any more [right column in Figs. 26(b)–26(e)]. Therefore, each of the road lanes could be considered as two different (and not connected) single-lane roads.

We have found that although no R → L lane-changing is possible on the single-lane road, within the range $q_{on,min} \leqslant q_{on} < q_{on,max}^{(1-lane)}$ free flow is indeed in a metastable state with respect to the F → S transition at the bottleneck [Figs. 30(a)–30(c)]. At a given $q_{in}$, the maximum on-ramp inflow-rate $q_{on,max}^{(1-lane)}$ determines the maximum capacity of automated-driving traffic on the single-lane road with the bottleneck: $C_{max} = q_{in} + q_{on,max}^{(1-lane)}$. When $q_{on} > q_{on,max}^{(1-lane)}$, then after a time delay $T^{(B)}$, which is a decreasing on-ramp inflow-rate function, the F → S transition occurs spontaneously at the bottleneck [Fig. 30(d)].

Thus, the minimum on-ramp inflow-rate $q_{on,min}$ of free-flow metastability with respect to the lane-asymmetric F → S transition at the bottleneck on two-lane road is determined by the minimum on-ramp inflow-rate $q_{on,min}$ of free-flow metastability on single-lane road with the same bottleneck. To explain this result, we should recall that in three-phase traffic theory [103–105], the term *over-acceleration* determines driver acceleration behaviors associated with a time delay in acceleration that causes free-flow metastability with respect to an F → S transition at a bottleneck. In Helly's model (1), (2) there is a time delay in acceleration. For this reason, it is not surprising that Helly's model (1), (2) shows over-acceleration on the single-lane road. However, the effect of this over-acceleration is practically insignificant: the range of the free-flow metastability on single-lane road is only $q_{on,max}^{(1-lane)} - q_{on,min} \approx 5$ vehicles/h [Fig. 28(d)].[18]

### D. Effect of desired time headway of automated vehicles

The basic result about the metastability of free flow with respect to the F → S transition at the bottleneck remains under a wide range of the desired time headway $\tau_d$ of automated vehicles. However, as shown in Fig. 31, the increase in $\tau_d$ to 1.5 s leads to a considerable decrease in the flow rate $q_{in}$ at which the metastability of free flow is realized.

## V. TRANSITIONS BETWEEN THE THREE PHASES IN AUTOMATED-DRIVING VEHICULAR TRAFFIC

Wide moving jams can emerge in synchronized flow. We have found that features of the jams are qualitatively almost the same as well-known for human-driving traffic. Thus, we present a simplified analysis of wide moving jams for model of Sec. IV C, when due to the use of condition (12) synchronized flow and wide moving jams can emerge in the right road lane only.

For a study of very low speed states in automated-driving vehicular traffic, we should note that in Eq. (1), when the speed $v \to 0$, the optimal gap between vehicles $g_{opt}$ (2) tends also to zero: $g_{opt} \to 0$. However, even when all vehicles are in standstill, the space gap between vehicles should be larger than zero. Therefore, when the vehicle speed decreases below some low speed denoted by $v_{min}$, in formula (2) we should add some additional space gap denoted by $g_{min}$ to which the space gap $g$ between automated vehicles tends when the speed $v \to 0$; therefore, formula (2) is replaced by a known formula

$$g_{opt} = \begin{cases} v\tau_d & \text{at } v \geqslant v_{min}, \\ g_{min} + v(\tau_d - \tau_{min}) & \text{at } v < v_{min}, \end{cases} \tag{13}$$

where $\tau_{min} = g_{min}/v_{min}$; $g_{min}$ and $v_{min}$ are constants.

We have found that in automated-driving traffic either a spontaneous S → J transition (Fig. 32) or induced S → J transition (Fig. 33) can be realized. Vehicle trajectories 1, 2, and 3 in Figs. 32(c) and 32(d) show a typical example of a time-development of an emergent wide moving jam (marked by "jam1") during the spontaneous S → J transition. The dynamics of the induced S → J transition [Figs. 33(a) and 33(b)] as well as a time-dependence of the speed of vehicle 4 propagating through the induced wide moving jam (marked by "jam2") show a possible coexistence of all three phases F, S, and J in automated-driving traffic [Fig. 33(c)] that is qualitatively very similar to that known for human-driving traffic. In addition with S → J transitions, a wide moving jam can be induced in free flow (induced F → J transition) (Fig. 34).

As in human-driving traffic, there are characteristic parameters of the downstream front propagation of a wide moving jam in automated-driving traffic that do not depend on initial

[18]Note that for Helly's model (1), (2) with $\tau_d = 1.5$ s, we have found $q_{on,max}^{(1-lane)} - q_{on,min} \approx 10$ vehicles/h.

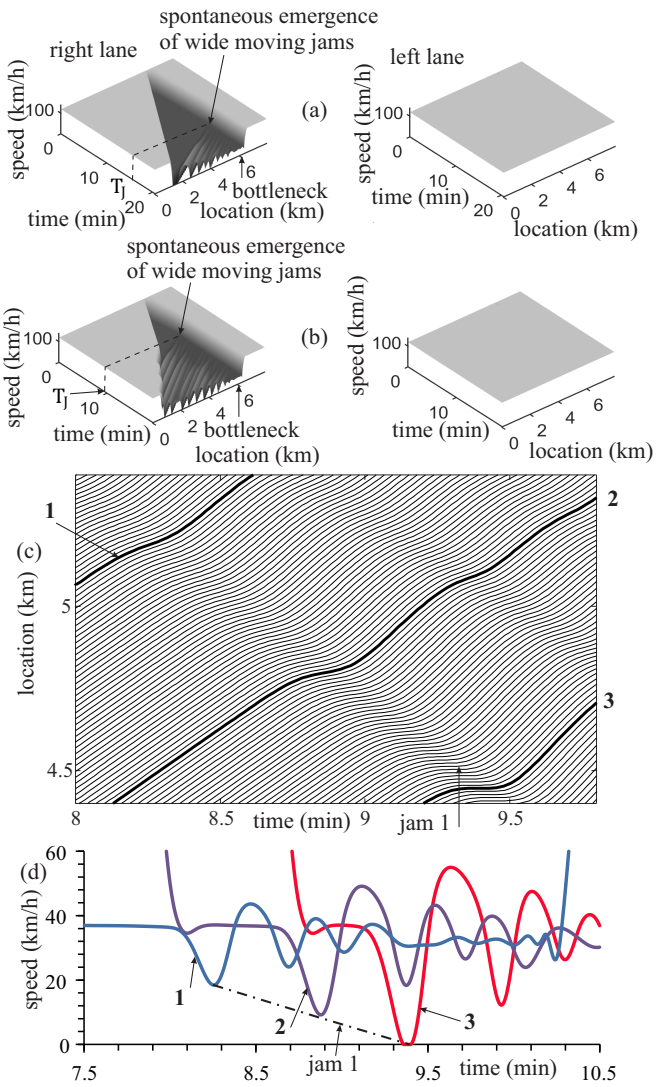


FIG. 32. Simulations of spontaneous S → J transition in model of Sec. IV C with the use of Eq. (13). Speed in space and time in the right lane (left column) and left lane (right column) at different $q_{on}$ at the same flow rate $q_{in} = 2571$ (vehicles/h)/lane as that in Fig. 3: (a) $q_{on} = 900$ vehicles/h. (b) $q_{on} = 940$ vehicles/h. (c) Vehicle trajectories in the right lane for a part of (b). (d) Time-functions of speeds of vehicles 1, 2, and 3 shown in panel (c). In Eq. (13), $v_{min} = 36$ km/h, $g_{min} = 3$ m. In panels (a), (b), first after a very short time delay $T^{(B)}$ [see Fig. 28(a)] a spontaneous F → S transition occurs; later in synchronized flow after a time delay denoted by $T_J$ spontaneous emerge of wide moving jams (S → J transition) is realized. Other model parameters are the same as those in Fig. 26.

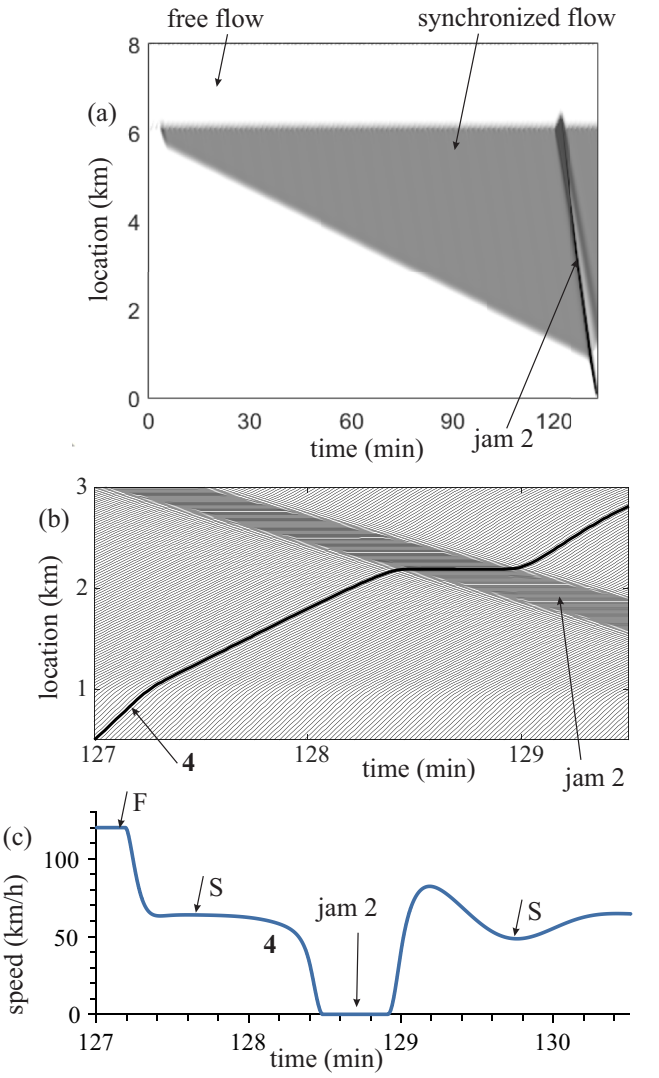


FIG. 33. Simulations of coexistence of the three phases F, S, and J with the use of a sequence of induced F → S and S → J transitions in model of Sec. IV C with the use of Eq. (13) at the same flow rate $q_{in} = 2571$ (vehicles/h)/lane as that in Fig. 3. (a) Speed data in space and time in the right lane presented by regions with variable shades of gray [shades of gray vary from white to black when the speed decreases from 120 km/h (white) to 0 km/h (black)]. $q_{on} = 400$ vehicles/h; for induced F → S transition, $T_{ind} = 3$ min, $\Delta q_{on} = 500$ vehicles/h, $\Delta t = 1$ min; for induced S → J transition, $T_{ind} = 120$ min, $\Delta q_{on} = 800$ vehicles/h, $\Delta t = 2$ min. (b) Vehicle trajectories in the right lane for a part of (a). (c) Time-function of speed of vehicle 4 in panel (b). Wide moving jam (J) is marked by "jam2", F—free flow, S—synchronized flow. Other model parameters are the same as those in Fig. 32.

conditions. The characteristic jam parameters presented by a line J in Fig. 35 are: (i) the velocity of the upstream propagation of the downstream jam front $v_g$, (ii) the flow rate $q_{out}$ and (iii) the density $\rho_{min}$ in the jam outflow (when free flow is built in this jam outflow) as well as (iv) the density within the jam $\rho_{max}$.

States of free flow, synchronized flow, and wide moving jams build together a double-Z (2Z) characteristic for phase transitions in automated-driving vehicular traffic (Fig. 36). At a given $q_{in}$, there is some maximum on-ramp inflow-rate $q_{on}$ denoted by $q^{(J)}_{on,max}$ (Fig. 36). The condition $q_{on} = q^{(J)}_{on,max}$ separates metastable synchronized flow at $q_{on} \leqslant q^{(J)}_{on,max}$ and unstable synchronized flow at $q_{on} > q^{(J)}_{on,max}$, when after a time delay $T_J$ a spontaneous S → J transition is realized (Fig. 32). The larger the difference $q_{on} - q^{(J)}_{on,max}$, the shorter the time delay $T_J$ of the S → J transition [Figs. 32(a) and 32(b)].

The 2Z characteristic shows (Fig. 36) that any phase transitions between the three phases F, S, and J are possible in a

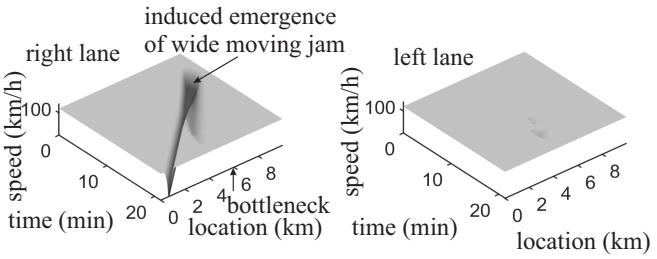


FIG. 34. Simulations of induced F → J transition in model of Sec. IV C with condition (13). Speed in space and time in the right lane (left column) and left lane (right column) at $q_{in} = 2880$ (vehicles/h)/lane and $q_{on} = 0$; for induced F → J transition, $T_{ind} =$ 3 min, $\Delta q_{on} = 1200$ vehicles/h, $\Delta t = 2$ min. Other model parameters are the same as those in Fig. 32.

broad range of the flow rate in automated-driving vehicular traffic on two-lane road at the bottleneck.

## VI. DISCUSSION

We have shown that traffic on a two-lane road with a bottleneck that consists of 100% string-stable automated ve-

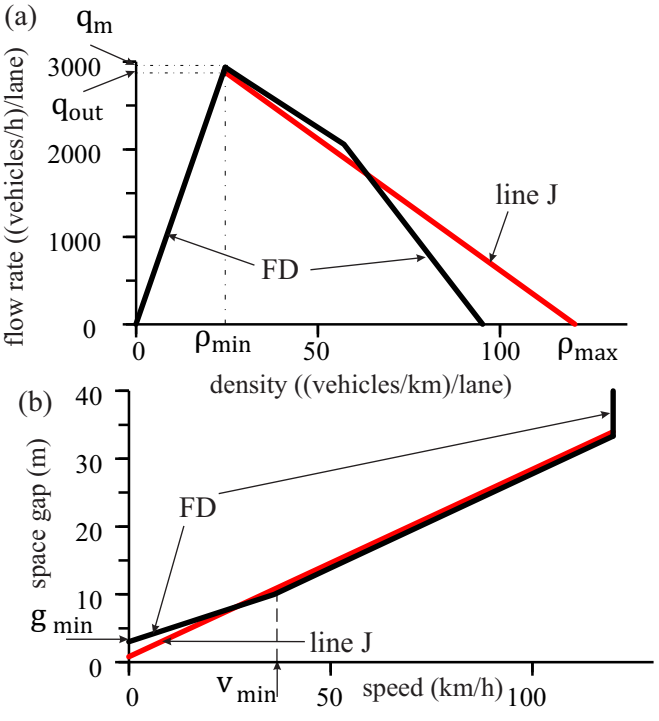


FIG. 35. Fundamental diagrams for hypothetical steady states (curves FD) and line J in the flow–density plane (a) and in the space-gap–speed plane (b). Model of Sec. IV C with the use of (13). The maximum flow rate on FD is $q_m = 3600/[\tau_d + (d/v_{free})] \approx$ 2939 (vehicles/h)/lane. Characteristics of line J calculated for the wide moving jam in Fig. 34 during the jam propagation in free flow are $v_g = 30$ km/h, $q_{out} = 2893$ (vehicles/h)/lane, $\rho_{min} = 24.5$ (vehicles/km)/lane, $\rho_{max} = 120.6$ (vehicles/km)/lane. Other model parameters are the same as those in Fig. 32.

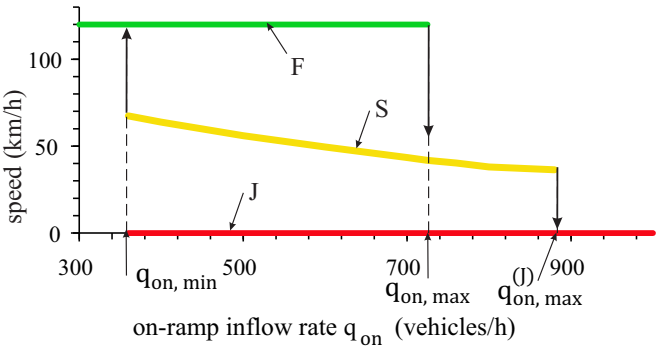


FIG. 36. Double-Z (2Z) characteristic for transitions between the three phases F, S, and J in automated-driving vehicular traffic: On-ramp inflow-rate function of average speed within the phases F, S, and J. Model of Sec. IV C with the use of (13) at $q_{in} = 2571$ (vehicles/h)/lane of Fig. 3. $q^{(J)}_{on,max} = 880$ vehicles/h. Other model parameters are the same as those in Figs. 28 and 32.

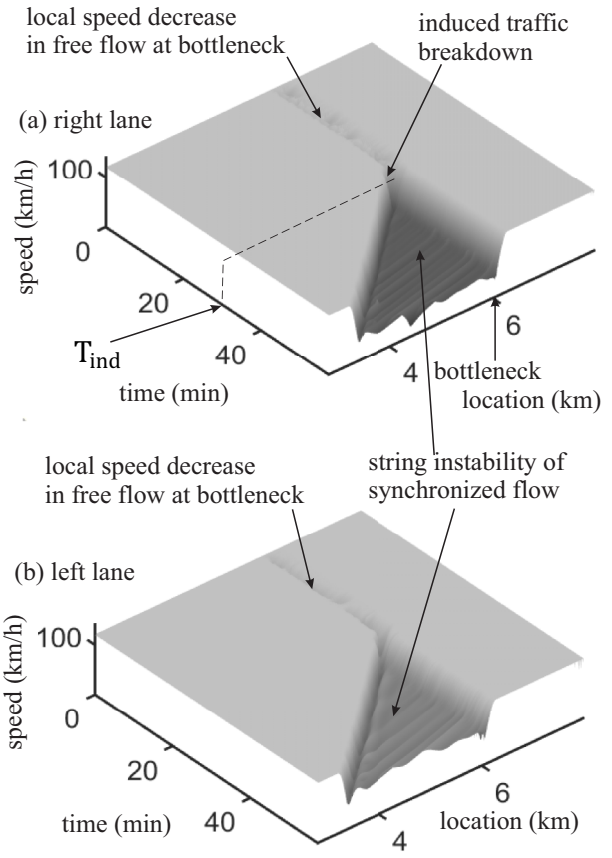


FIG. 37. Simulations of F → S transition on two-lane road with bottleneck of model of Sec. II A with the use of Eq. (13), however, when condition (3) for string stability is *not* satisfied: Speed in space and time in the right lane (left) and left lane (right) at $q_{in} = 2571$ (vehicles/h)/lane of Fig. 3. Induced F → S transition simulated as in Fig. 4. $\tau_d = 1$ s, $K_1 = 0.3$ s$^{-2}$, $K_2 = 0.75$ s$^{-1}$, $q_{on} = 650$ vehicles/h, $T_{ind} = 30$ min, $\Delta q_{on} = 250$ vehicles/h, $\Delta t = 2$ min. Other model parameters are the same as those in Fig. 3.

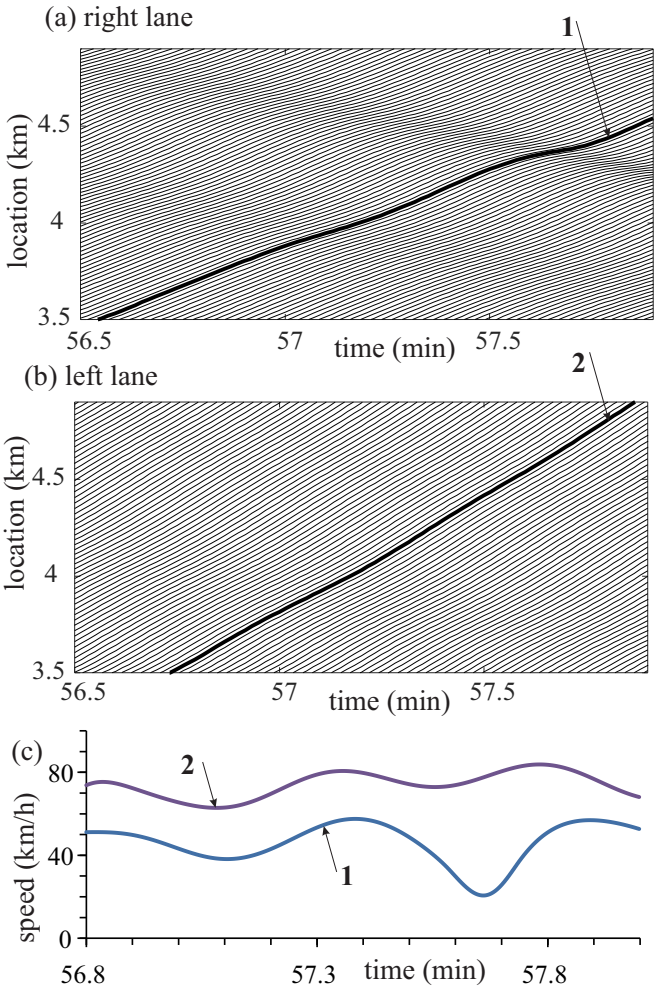


FIG. 38. Continuation of Fig. 37. String instability of synchronized flow: (a), (b) Simulated vehicle trajectories in synchronized flow in the right lane (a) and left lane (b) at time $t > T_{\rm ind} + \Delta t$. (c) Time-functions of speeds of vehicle 1 in the right lane and vehicle 2 in the left lane marked by the same numbers in panels (a), (b).

hicles moving in a road lane in accordance with the classical Helly's model [137] is described in the framework of the three-phase traffic theory in which traffic breakdown is an F → S transition that exhibits the nucleation nature. Does this basic paper result remain when vehicle platoons are string-unstable (Sec. VI A) or when a qualitatively different model for automated-driving vehicles is used (Sec. VI B)?

### A. F → S transition at bottleneck in automated-driving vehicular traffic under string-unstable conditions

The basic paper result about the nucleation nature of traffic breakdown (F → S transition) of the three-phase traffic theory is valid for both string-stable and string-unstable automated-driving vehicular traffic (Fig. 37). In free flow, when the speed is equal to $v_{\rm free}$, the mean time headway between vehicles $\tau_{\rm mean}^{\rm (free)}$ is longer than the desired value $\tau_{\rm d}$ in Eqs. (1), (2) (at model parameters used in Fig. 37, we get $\tau_{\rm mean}^{\rm (free)} = (3600/q_{\rm in}) - (d/v_{\rm free}) \approx 1.175$ s, whereas $\tau_{\rm d} = 1$ s).

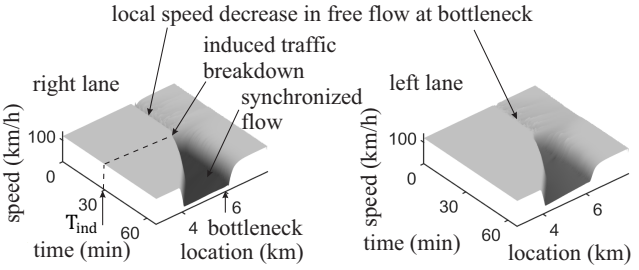


FIG. 39. Nucleation features of F → S transition in automated-driving traffic consisting of 100% TPACC-vehicles (14) under the use of lane-changing and bottleneck models of Sec. II A: Speed in space and time in the right lane (left column) and left lane (right column). $\tau_{\rm p} = 1.3$ s, $\tau_{\rm G} = 1.4$ s, $\tau_{\rm safe} = 1$ s, $K_1 = 0.3$ s$^{-2}$, $K_{\Delta v} = K_2 = 0.6$ s$^{-1}$, $\tau_1 = \tau_2 = 0.5$ s, $q_{\rm in} = 2000$ (vehicles/h)/lane, $q_{\rm on} = 700$ vehicles/h, $T_{\rm ind} = 30$ min, $\Delta q_{\rm on} = 200$ vehicles/h, $\Delta t = 2$ min. Other parameters are the same as those in Fig. 3.

Therefore, no long enough vehicle platoons in which automated vehicles moves at time headway $\tau_{\rm d}$ can be built in free flow at the bottleneck: No string instability occurs in free flow. This explains why basic features of the free-flow metastability with respect to the F → S transition at the bottleneck remain qualitatively the same as those found in Secs. II–V for string-stable automated vehicles.

Contrary to free flow, in synchronized flow resulting from the F → S transition at the bottleneck very long vehicle platoons in which automated vehicles moves at time headway $\tau_{\rm d}$ can be built. For this reason, in synchronized flow the string instability is realized (Fig. 38).[19]

### B. Automated-driving traffic based on three-phase adaptive cruise control (TPACC)

The basic result of the paper about the nucleation nature of traffic breakdown (F → S transition) of the three-phase traffic theory remains when a qualitatively different model for automated-driving vehicles is used. In Fig. 39, automated-driving traffic based on three-phase adaptive cruise control (TPACC) is simulated. The TPACC-model reads as

[19]We note that there are no collisions between vehicles in all simulations of string-stable automated vehicles presented in Secs. II–V (as well as in Sec. VI B below). There are also no collisions between automated vehicles during time interval $T_{\rm ind} \leqslant t \leqslant 58$ min of the development of the string instability in synchronized flow (Figs. 37 and 38). However, if under model parameters used in Fig. 37 a further growth of speed waves due to the development of the string instability in synchronized flow at $t > 58$ min is studied (not shown in the paper), then collisions between vehicles can be found at very low speeds; in particular, the collisions occur by R → L lane-changing. For this reason, for a study of the time-development of the string instability in synchronized flow on a two-lane road with the bottleneck rather than the simple model of Sec. II A another model should be used; such a detailed study of the string instability in synchronized flow is out of the scope of this paper.

follows [136,140]:

$$a^{(\mathrm{TPACC})} = \begin{cases} K_{\Delta v}\Delta v & \text{at } g_{\mathrm{safe}} \leqslant g \leqslant G, \\ K_1(g - g_{\mathrm{opt}}) + K_2\Delta v & \text{at } g < g_{\mathrm{safe}} \text{ or } g > G, \end{cases} \tag{14}$$

where $K_{\Delta v}$ is a constant dynamic coefficient ($K_{\Delta v} > 0$), $G$ is a synchronization space gap, $G = v\tau_{\mathrm{G}}$, $\tau_{\mathrm{G}}$ is a synchronization time headway, $g_{\mathrm{safe}}$ is a safe space gap, $g_{\mathrm{safe}} = v\tau_{\mathrm{safe}}$, $\tau_{\mathrm{safe}}$ is a safe time headway, $g_{\mathrm{opt}}$ is given by Eq. (13) when in this formula $\tau_{\mathrm{d}}$ is replaced by model parameter $\tau_{\mathrm{p}}$ that satisfies condition $\tau_{\mathrm{p}} < \tau_{\mathrm{G}}$. In contrast with the model (1), (13), in the TPACC-model (14) there is an indifference zone for car-following when time headway is between $\tau_{\mathrm{safe}}$ and $\tau_{\mathrm{G}}$, i.e., there is no fixed desired time headway between vehicles in TPACC-vehicle platoons. For this reason, as shown in Ref. [136], there is no string-instability in TPACC-vehicle platoons.

Simulations show that nucleation features of the F → S transition in automated-driving based on the TPACC-model (14) are qualitatively the same as those found in Secs. II–V for string-stable automated vehicular traffic with the use of Helly's model (1), (2). However, there are some qualitative differences in synchronized flow behavior caused by the indifference zone for car-following in the TPACC-model (14). For example, while the velocity of the upstream synchronized flow front for Helly's model (1), (2) is almost time-independent (Fig. 4), this velocity can depend on time in the TPACC-model (14) (Fig. 39). A more detailed consideration of three-phase traffic theory for automated-driving traffic based on the TPACC-model that could be an interesting subject of scientific investigations is out of the scope of this paper.

### C. Conclusions

(1) The nucleation nature of traffic breakdown (F → S transition) at a highway bottleneck, which is the basic feature of the three-phase traffic theory for human-driving traffic, has been revealed for vehicular traffic consisting of 100% of automated-driving vehicles moving on a two-lane road with an on-ramp bottleneck. As long as lane-changing in free flow ensures a distribution of the on-ramp inflow between road lanes, this basic result remains in a broad range of model parameters of automated-driving vehicles.

(2) We have found that there is a discontinuity in the rate of lane-changing from the right lane (neighborhood lane to on-ramp) to the left lane (passing lane) (denoted as R → L lane-changing). In its turn, this causes the discontinuity in the over-acceleration rate: The rate of over-acceleration in free flow is larger than it is in synchronized flow.

(3) The cause of the nucleation nature of traffic breakdown (F → S transition) in automated-driving vehicular traffic at a bottleneck is the discontinuity in the over-acceleration rate together with a spatiotemporal competition between over-acceleration and speed adaptation. A larger rate of over-acceleration in free flow causes the maintenance of free flow at the bottleneck; contrarily, a lower rate of over-acceleration in synchronized flow causes the maintenance of synchronized flow at the bottleneck.

(4) Through the spatiotemporal competition between over-acceleration and speed adaptation caused by lane-changing, at any time instant there is a range of highway capacities between some minimum and maximum capacities; within the capacity range, an F → S transition can be induced; however, when the maximum capacity is exceeded, then after some time-delay a spontaneous F → S transition occurs at the bottleneck. All three-phases [free flow (F), synchronized flow (S), and wide moving jam (J)] can coexist each other in automated-driving traffic. A diverse variety of phase transitions, which can occur between the phases F, S, and J, determine the spatiotemporal dynamics of automated-driving vehicular traffic.

(5) The discontinuous character of over-acceleration caused by lane-changing is the universal physical feature of vehicular traffic. The three-phase traffic theory is the framework for both human-driving and automated-driving vehicular traffic. Therefore, we can assume that the three-phase traffic theory is also the framework for a mixed traffic consisting of a random distribution of human-driving and automated-driving vehicles. Three-phase traffic theory of mixed traffic that is out of the scope of this paper could be a very interesting task for further traffic studies.

### ACKNOWLEDGMENTS

I thank Sergey Klenov for help in simulations and useful suggestions. I thank our partners for their support in the project "LUKAS–Lokales Umfeldmodell für das Kooperative, Automatisierte Fahren in komplexen Verkehrssituationen," funded by the German Federal Ministry for Economic Affairs and Climate Action.

[1] M. J. Lighthill and G. B. Whitham, Proc. R. Soc. A **229**, 281 (1955).
[2] P. I. Richards, Oper. Res. **4**, 42 (1956).
[3] A. D. May, *Traffic Flow Fundamentals* (Prentice-Hall, Hoboken, NJ, 1990).
[4] C. F. Daganzo, Transp. Res. B **28**, 269 (1994); **29**, 79 (1995); *Fundamentals of Transportation and Traffic Operations* (Elsevier Science, New York, 1997).
[5] *Highway Capacity Manual*, 6th ed., National Research Council (Transportation Research Board, Washington, DC, 2016).
[6] R. P. Roess and E. S. Prassas, *The Highway Capacity Manual: A Conceptual and Research History* (Springer, Berlin, 2014).
[7] Daiheng Ni, *Traffic Flow Theory: Characteristics, Experimental Methods, and Numerical Techniques* (Elsevier, Amsterdam, 2015).
[8] R. E. Chandler, R. Herman, and E. W. Montroll, Oper. Res. **6**, 165 (1958).
[9] R. Herman, E. W. Montroll, R. B. Potts, and R. W. Rothery, Oper. Res. **7**, 86 (1959).

[10] D. C. Gazis, R. Herman, and R. B. Potts, Oper. Res. **7**, 499 (1959).

[11] D. C. Gazis, R. Herman, and R. W. Rothery, Oper. Res. **9**, 545 (1961).

[12] E. Kometani and T. Sasaki, J. Oper. Res. Soc. Jpn. **2**, 11 (1958).

[13] E. Kometani and T. Sasaki, Oper. Res. **7**, 704 (1959).

[14] E. Kometani and T. Sasaki, J. Oper. Res. Soc. Jpn. **3**, 176 (1961).

[15] E. Kometani and T. Sasaki, in *Theory of Traffic Flow*, edited by R. Herman (Elsevier, Amsterdam, 1961), pp. 105–119.

[16] G. F. Newell, Oper. Res. **9**, 209 (1961); Transp. Res. B **36**, 195 (2002).

[17] G. F. Newell, in *Proceedings of the 2nd International Symposium on Road Traffic Flow* (OECD, London 1963), pp. 73–83.

[18] P. G. Gipps, Trans. Res. B **15**, 105 (1981).

[19] K. Nagel and M. Schreckenberg, J. Phys. I France **2**, 2221 (1992).

[20] M. Bando, K. Hasebe, A. Nakayama, A. Shibata, and Y. Sugiyama, Jpn. J. Appl. Math. **11**, 203 (1994); Phys. Rev. E **51**, 1035 (1995).

[21] D. Chowdhury, L. Santen, and A. Schadschneider, Phys. Rep. **329**, 199 (2000).

[22] D. Helbing, Rev. Mod. Phys. **73**, 1067 (2001).

[23] T. Nagatani, Rep. Prog. Phys. **65**, 1331 (2002).

[24] K. Nagel, P. Wagner, and R. Woesler, Oper. Res. **51**, 681 (2003).

[25] M. Saifuzzaman and Z. Zheng, Transp. Res. C **48**, 379 (2014).

[26] A. Schadschneider, D. Chowdhury, and K. Nishinari, *Stochastic Transport in Complex Systems* (Elsevier Science, New York, 2011).

[27] M. Treiber and A. Kesting, *Traffic Flow Dynamics* (Springer, Berlin, 2013).

[28] W. D. Ashton, *The Theory of Traffic flow* (Methuen & Co., London/John Wiley & Sons, New York, NY, 1966).

[29] D. L. Gerlough and M. J. Huber, *Traffic Flow Theory Special Report 165* (Transp. Res. Board, Washington DC, 1975).

[30] D. C. Gazis, *Traffic Theory* (Springer, Berlin, 2002).

[31] J. Barceló (ed.), *Fundamentals of Traffic Simulation* (Springer, Berlin, 2010).

[32] L. Elefteriadou, *An Introduction to Traffic Flow Theory* (Springer, Berlin, 2014).

[33] F. Kessels, *Traffic Flow Modelling* (Springer, Berlin, 2019).

[34] B. S. Kerner and P. Konhäuser, Phys. Rev. E **48**, R2335 (1993); **50**, 54 (1994).

[35] P. A. Ioannou and E. B. Kosmatopoulos, Adaptive control, in *Wiley Encyclopedia of Electrical and Electronics Engineering*, edited by John G. Webster (John Wiley & Sons, New York, 2000).

[36] P. A. Ioannou and C. C. Chien, IEEE Trans. Veh. Technol. **42**, 657 (1993).

[37] W. Levine and M. Athans, IEEE Trans. Automat. Contr. **11**, 355 (1966).

[38] C.-Y. Liang and H. Peng, Veh. Syst. Dyn. **32**, 313 (1999).

[39] C.-Y. Liang and H. Peng, JSME Jnt. J. Ser. C **43**, 671 (2000).

[40] D. Swaroop and J. K. Hedrick, IEEE Trans. Automat. Contr. **41**, 349 (1996); D. Swaroop, J. K. Hedrick, and S. B. Choi, IEEE Trans. Veh. Technol. **50**, 150 (2001).

[41] P. Varaiya, IEEE Trans. Automat. Contr. **38**, 195 (1993).

[42] T.-W. Lin, S.-L. Hwang, and P. Green, Safety Sci. **47**, 620 (2009).

[43] J.-J. Martinez and C. Canudas-do-Wit, IEEE Trans. Cont. Syst. Tech. **15**, 246 (2007).

[44] J. Van Brummelen, M. O'Brien, D. Gruyer, and H. Najjaran, Transp. Res. C **89**, 384 (2018).

[45] S. E. Shladover, Veh. Syst. Dyn. **24**, 551 (1995); S. E. Shladover, D. Su, and X.-T. Lu, Transp. Res. Rec. **2324**, 63 (2012).

[46] R. Rajamani, *Vehicle Dynamics and Control*, Mechanical Engineering Series (Springer US, Boston, MA, 2012).

[47] L. C. Davis, Phys. Rev. E **69**, 066110 (2004).

[48] L. C. Davis, Physica A **405**, 128 (2014).

[49] L. C. Davis, Physica A **451**, 320 (2016); **368**, 541 (2006); **361**, 606 (2006); **379**, 274 (2007); **387**, 6395 (2008).

[50] R. Schmitz, M. Torrent-Moreno, H. Hartenstein, and W. Effelsberg, in *Proceedings of the 29th Annual IEEE International Conference on Local Computer Networks* (IEEE, Tampa, FL, 2004), pp. 594–601.

[51] J. Maurer, T. Fuegen, and W. Wiesbeck, in *Proceedings of the 11th European Wireless Conference 2005: Next Generation wireless and Mobile Communications and Services* (VDE-Verlag, Berlin, 2006), pp. 1–7.

[52] Q. Chen, D. Jiang, V. Taliwal, and L. Delgrossi, in *Proceedings of the 3rd International Workshop on Vehicular ad hoc Networks (VANET'06)* (ACM, New York, 2006), pp. 50–56.

[53] T.-H. Wang, S. Manivasagam, M. Liang, B. Yang, W. Zeng, and R. Urtasun, in *Proceedings of the European Conference on Computer Vision (ECCV'20)*, Lecture Notes in Computer Science Vol. 12347, edited by A. Vedaldi, H. Bischof, T. Brox, and J.-M. Frahm (Springer, Cham, 2020).

[54] *Vehicular Communications and Networks*, edited by W. Chen (Woodhead Publishings, Cambridge, UK, 2015).

[55] S. Darbha and K. R. Rajagopal, Transp. Res. C **7**, 329 (1999).

[56] G. Marsden, M. McDonald, and M. Brackstone, Transp. Res. C **9**, 33 (2001).

[57] H. Krishnan, Transp. Res. Rec. **1748**, 167 (2001).

[58] J. VanderWerf, S. E. Shladover, M. Miller, and N. Kourjanskaia, Transp. Res. Rec. **1800**, 78 (2002).

[59] P. Y. Li and A. Shrivastava, Transp. Res. C **10**, 275 (2002).

[60] S. Kikuchi, N. Uno, and M. Tanaka, J. Transp. Eng. **129**, 146 (2003).

[61] A. Bose and P. Ioannou, Transp. Res. C **11**, 439 (2003).

[62] H. Suzuki, JSAE Rev. **24**, 403 (2003).

[63] J. Zhou and H. Peng, IEEE Trans. Intell. Transp. Syst. **6**, 229 (2005).

[64] B. van Arem, C. J. G. van Driel, and R. Visser, IEEE Trans. ITS **7**, 429 (2006).

[65] M. Treiber and D. Helbing, Automatisierungstechnik **49**, 478 (2001); A. Kesting, M. Treiber, M. Schönhof, and D. Helbing, Transp. Res. Rec. **2000**, 16 (2007); Transp. Res. C **16**, 668 (2008); A. Kesting, M. Treiber, and D. Helbing, Philos. Trans. R. Soc. A **368**, 4585 (2010).

[66] D. Ngoduy, Transportmetrica **8**, 43 (2012); Commun. Nonlinear Sci. Numer. Simul. **18**, 2838 (2013).

[67] A. I. Delis, I. K. Nikolos, and M. Papageorgiou, Comput. Math. Appl. **70**, 1921 (2015); I. A. Ntousakis, I. K. Nikolos, and M. Papageorgiou, Transp. Res. Procedia **6**, 111 (2015); C. Roncoli, M. Papageorgiou, and I. Papamichail, Transp. Res. C

**57**, 241 (2015); G. Perraki, C. Roncoli, I. Papamichail, and M. Papageorgiou, *ibid.* **92**, 456 (2018).
[68] A. Talebpour and H. S. Mahmassani, Transp. Res. C **71**, 143 (2016).
[69] R. Wang, Y. Li, and D. B. Work, Transp. Res. C **78**, 95 (2017).
[70] M. Mamouei, I. Kaparias, and G. Halikias, Transp. Res. C **92**, 27 (2018).
[71] G. Sharon, M. W. Levin, J. P. Hanna, T. Rambha, S. D. Boyles, and P. Stone, Transp. Res. C **84**, 142 (2017).
[72] Y. Han and S. Ahn, Transp. Res. B **107**, 146 (2018); D. Chen, S. Ahn, M. Chitturi, and D. A. Noyce, *ibid.* **100**, 196 (2017).
[73] M. Zhou, X. Qu, and S. Jin, IEEE Trans. ITS **18**, 1422 (2017).
[74] M. Klawtanong and S. Limkumnerd, Physica A **542**, 123412 (2020).
[75] G. Zhang, Y. Zhang, D.-B. Pan, and R.-J. Huang, Physica A **534**, 122029 (2019).
[76] H. B. Zhu, Y. J. Zhou, and W. J. Wu, Physica A **549**, 124337 (2020).
[77] J. Zhou and F. Zhu, Trans. Res. C **115**, 102614 (2020).
[78] Y. Zhou, S. Ahn, M. Wang, and S. Hoogendoorn, Transp. Res. B **132**, 152 (2020).
[79] D. Chen, A. Srivastava, S. Ahn, and T. Li, Transp. Res. C **113**, 293 (2020).
[80] Z. Zhong, E. E. Lee, M. Nejad, and J. Lee, Transp. Res. C **115**, 102611 (2020).
[81] F.-f. Zheng, C. Liu, X. Liu, S. E. Jabari, and L. Lu, Transp. Res. C **112**, 203 (2020).
[82] S. Jin, D.-H. Sun, M. Zhao, Y. Li, and J. Chen, Physica A **551**, 124217 (2020).
[83] Y. J. Zhou, H. B. Zhu, M. M. Guo, and J. L. Zhou, Physica A **540**, 122721 (2020).
[84] Z. Yao, R. Hu, Y. Wang, Y. Jiang, B. Ran, and Y. Chen, Physica A **533**, 121931 (2019).
[85] L. Ye and T. Yamamoto, Physica A **490**, 269 (2018); **512**, 588 (2018); **526**, 121009 (2019).
[86] W.-X. Zhu and H. M. Zhang, Physica A **496**, 274 (2018).
[87] Z. Wen-Xing and Z. Li-Dong, Physica A **492**, 2154 (2018).
[88] X. Chang, H. Li, J. Rong, X. Zhao, and A. Li, Physica A **557**, 124829 (2020).
[89] Y. Jiang, S. Wang, Z. Yao, B. Zhao, and Y. Wang, Physica A **582**, 126262 (2021); Z. Yao, Q. Gu, Y. Jiang, and B. Ran, *ibid.* **604**, 127857 (2022); Y. Jiang, S. Sun, F. Zhu, Y. Wu, and Z. Yao, *ibid.* **615**, 128557 (2023).
[90] K. Ma, H. Wang, and T. Ruan, Physica A **583**, 126301 (2021).
[91] R. Luo, Q. Gu, T. Xu, H. Hao, and Z. Yao, Physica A **597**, 127211 (2022).
[92] L. Ma, S. Qu, J. Ren, and X. Zhang, Math. Biosci. Eng. **20**, 2280 (2023).
[93] F. V. Monteiro and P. Ioannou, Transp. Res. C **151**, 104138 (2023).
[94] X. Li, Y. Xiao, X. Zhao, X. Ma, and X. Wang, Physica A **609**, 128368 (2023).
[95] Z. Gu, Z. Wang, Z. Liu, and M. Saberi, Transp. Res. C **138**, 103626 (2022).
[96] T. Vranken, B. Sliwa, C. Wietfeld, and M. Schreckenberg, Physica A **570**, 125792 (2021); T. Vranken and M. Schreckenberg, *ibid.* **589**, 126629 (2022).
[97] Ó. Silva, R. Cordera, E. González-González, and S. Nogués, Sci. Total Environ. **830**, 154615 (2022).
[98] J. Tanimoto, M. Futamata, and M. Tanaka, Chaos, Solitons Fractals **138**, 109861 (2020).
[99] R. Fu, Z. Li, Q. Sun, and C. Wang, Accident Anal. Preventi. **132**, 105260 (2019).
[100] B. S. Kerner, Trans. Res. Rec. **1678**, 160 (1999); in *Transportation and Traffic Theory*, edited by A. Ceder (Elsevier Science, Amsterdam, 1999), pp. 147–171; B. S. Kerner, Phys. World **12**, 25 (1999); Trans. Res. Rec. **1710**, 136 (2000); Net. Spat. Econ. **1**, 35 (2001); Phys. Rev. E **65**, 046138 (2002); Math. Comput. Model. **35**, 481 (2002).
[101] B. S. Kerner, J. Phys. A: Math. Gen. **33**, L221 (2000); in *Traffic and Granular Flow'99: Social, Traffic and Granular Dynamics*, edited by D. Helbing, H. J. Herrmann, M. Schreckenberg, and D. E. Wolf (Springer, Berlin, 2000), pp. 253–284; in *Traffic and Transportation Theory in the 21st Century*, edited by M. A. P. Taylor (Elsevier Science, Amsterdam, 2002), pp. 417–439; Transp. Res. Rec. **1802**, 145 (2002).
[102] B. S. Kerner, Phys. Rev. Lett. **81**, 3797 (1998); in *Proceedings of the 3rd International Symposium on Highway Capacity*, edited by R. Rysgaard (Road Directorate, Ministry of Transport, Denmark, 1998), pp. 621–641.
[103] B. S. Kerner, *The Physics of Traffic* (Springer, Berlin/New York, 2004).
[104] B. S. Kerner, *Introduction to Modern Traffic Flow Theory and Control* (Springer, Berlin/New York, 2009).
[105] B. S. Kerner, *Breakdown in Traffic Networks* (Springer, Berlin/New York, 2017).
[106] B. S. Kerner, *Understanding Real Traffic* (Springer, Cham, 2021).
[107] B. S. Kerner, in *Complex Dynamics of Traffic Management*, 2nd ed., edited by B. S. Kerner, Encyclopedia of Complexity and Systems Science Series (Springer, New York, 2019), pp. 21–77.
[108] B. S. Kerner, M. Koller, S. L. Klenov, H. Rehborn, and M. Leibel, Physica A **438**, 365 (2015).
[109] B. S. Kerner, H. Rehborn, R.-P. Schäfer, S. L. Klenov, J. Palmer, S. Lorkowski, and N. Witte, Physica A **392**, 221 (2013).
[110] B. S. Kerner and S. L. Klenov, J. Phys. A: Math. Gen. **35**, L31 (2002).
[111] B. S. Kerner, S. L. Klenov, and D. E. Wolf, J. Phys. A: Math. Gen. **35**, 9971 (2002).
[112] B. S. Kerner and S. L. Klenov, Phys. Rev. E **68**, 036130 (2003); J. Phys. A: Math. Gen. **37**, 8753 (2004); B. S. Kerner, Physica A **333**, 379 (2004); **355**, 565 (2005); B. S. Kerner and S. L. Klenov, J. Phys. A: Math. Gen. **39**, 1775 (2006); B. S. Kerner, S. L. Klenov, and A. Hiller, *ibid.* **39**, 2001 (2006); B. S. Kerner, S. L. Klenov, A. Hiller, and H. Rehborn, Phys. Rev. E **73**, 046107 (2006); B. S. Kerner, S. L. Klenov, and A. Hiller, Non. Dyn. **49**, 525 (2007); B. S. Kerner, Transp. Res. Rec. **1999**, 30 (2007); IEEE Trans. ITS **8**, 308 (2007); B. S. Kerner and S. L. Klenov, Phys. Rev. E **80**, 056101 (2009); Transp. Res. Rec. **2124**, 67 (2009); B. S. Kerner, J. Phys. A: Math. Theor. **41**, 215101 (2008); **44**, 092001 (2011); Phys. Rev. E **85**, 036110 (2012); in *Complex Dynamics of Traffic Management*, 2nd ed., edited by B. S. Kerner, Encyclopedia of Complexity and Systems Science Series (Springer, New York, 2019), pp. 387–500.

[113] L. C. Davis, Phys. Rev. E **69**, 016108 (2004); Physica A **388**, 4459 (2009); **389**, 3588 (2010); **391**, 1679 (2012).

[114] H. K. Lee, R. Barlović, M. Schreckenberg, and D. Kim, Phys. Rev. Lett. **92**, 238702 (2004); A. Pottmeier, C. Thiemann, A. Schadschneider, and M. Schreckenberg, in *Traffic and Granular Flow'05*, edited by A. Schadschneider, T. Pöschel, R. Kühne, M. Schreckenberg, and D. E. Wolf (Springer, Berlin, 2007), pp. 503–508; H.-K. Lee and B.-J. Kim, Physica A **390**, 4555 (2011).

[115] R. Jiang and Q.-S. Wu, J. Phys. A: Math. Gen. **37**, 8197 (2004); K. Gao, R. Jiang, S.-X. Hu, B.-H. Wang, and Q.-S. Wu, Phys. Rev. E **76**, 026105 (2007).

[116] X. G. Li, Z. Y. Gao, K. P. Li, and X. M. Zhao, Phys. Rev. E **76**, 016110 (2007).

[117] K. Hausken and H. Rehborn, *Game Theoretic Analysis of Congestion, Safety and Security*, Springer Series in Reliability Engineering (Springer, Berlin, 2015), pp. 113–141.

[118] I. Lubashevsky, *Physics of the Human Mind* (Springer, Berlin, 2017); I. Lubashevsky and K. Morimura, in *Complex Dynamics of Traffic Management*, 2nd ed., edited by B. S. Kerner, Encyclopedia of Complexity and Systems Science Series, (Springer, New York, 2019), pp. 559–592.

[119] J.-f. Tian, C. Zhu, and R. Jiang, in *Complex Dynamics of Traffic Management*, 2nd ed., edited by B. S. Kerner, Encyclopedia of Complexity and Systems Science Series (Springer, New York, NY, 2019), pp. 313–342; S. Zhou, S. Ling, C. Zhu, and J.-f. Tian, Physica A **596**, 127162 (2022).

[120] J.-W. Zeng, Y.-S. Qian, Z. Lv, F. Yin, L. Zhu, Y. Zhang, and D. Xu, Physica A **574**, 125918 (2021); J.-W. Zeng, Y.-S. Qian, S.-B. Yu, and X.-T. Wei, *ibid.* **530**, 121567 (2019).

[121] H.-T. Zhao, L. Lin, C.-P. Xu, Z.-X. Li, and X. Zhao, Physica A **553**, 124213 (2020).

[122] J. J. Wu, H. J. Sun, and Z. Y. Gao, Phys. Rev. E **78**, 036103 (2008).

[123] H. Yang, J. Lu, X.-J. Hu, and J. Jiang, Physica A **392**, 4009 (2013).

[124] H. Yang, X. Zhai, and C. Zheng, Physica A **509**, 567 (2018).

[125] F. Siebel and W. Mauser, Phys. Rev. E **73**, 066108 (2006).

[126] F. Rempe, P. Franeck, U. Fastenrath, and K. Bogenberger, Transp. Res. C **85**, 644 (2017).

[127] H. Rehborn and S. L. Klenov, in *Encyclopedia of Complexity and System Science*, edited by R. A. Meyers (Springer, Berlin, 2009), pp. 9500–9536; H. Rehborn, S. L. Klenov, and M. Koller, in *Complex Dynamics of Traffic Management*, 2nd ed., edited by B. S. Kerner, Encyclopedia of Complexity and Systems Science Series (Springer, New York, 2019), pp. 501–557.

[128] H. Rehborn, S. L. Klenov, and J. Palmer, Physica A **390**, 4466 (2011); H. Rehborn and J. Palmer, in *Proceedings of the 2008 Intelligent Vehicles Symposium* (IEEE, New York, 2008), pp. 186–191; H. Rehborn, S. L. Klenov, and J. Palmer, in *Proceedings of the 4th IEEE Intelligent Vehicle Symposium* (IEEE, New York, 2011), pp. 19–24; H. Rehborn and M. Koller, J. Adv. Transp. **48**, 1107 (2014).

[129] H. Rehborn, M. Koller, and S. Kaufmann, *Data-Driven Traffic Engineering: Understanding of Traffic and Applications based on Three-Phase Traffic Theory* (Elsevier, Amsterdam, 2021).

[130] Y.-S. Qian, X. Feng, and J.-W. Zeng, Physica A **479**, 509 (2017).

[131] J. P. L. Neto, M. L. Lyra, and C. R. da Silva, Physica A **390**, 3558 (2011).

[132] X.-j. Hu, H. Liu, X. Hao, Z. Su, and Z. Yang, Physica A **563**, 125495 (2021); X.-j. Hu, F. Zhang, J. Lu, M.-y. Liu, Y.-f. Ma, and Q. Wan, *ibid.* **527**, 121176 (2019); X.-j. Hu, X.-t. Hao, H. Wang, Z. Su, and F. Zhang, *ibid.* **545**, 123725 (2020); X.-j. Hu, L.-q. Qiao, X.-t. Hao, C.-x. Lin, and T.-h. Liu, *ibid.* **605**, 127962 (2022).

[133] D.-J. Fu, Q.-L. Li, R. Jiang, and B.-H. Wang, Physica A **559**, 125075 (2020); Q.-L. Li, J.-X. Wang, L.-L. Ye, R. Jiang, and B.-H. Wang, Int. J. Mod. Phys. C (2023), doi:10.1142/S0129183123501206.

[134] R. Borsche, M. Kimathi, and A. Klar, Comput. Math. Appl. **64**, 2939 (2012).

[135] V. Wiering, S. L. Klenov, B. S. Kerner, and M. Schreckenberg, Phys. Rev. E **106**, 054306 (2022).

[136] B. S. Kerner, Phys. Rev. E **97**, 042303 (2018); Physica A **562**, 125315 (2021); Procedia Computer Science **130**, 785 (2018); in *Complex Dynamics of Traffic Management*, 2nd ed., edited by B. S. Kerner, Encyclopedia of Complexity and Systems Science Series, (Springer, New York, 2019), pp. 343–385.

[137] W. Helly, in *Proceedings of the Symposium on Theory of Traffic Flow*, Research Laboratories, General Motors (Elsevier, Amsterdam, 1959), pp. 207–238.

[138] K. Nagel, D. E. Wolf, P. Wagner, and P. Simon, Phys. Rev. E **58**, 1425 (1998).

[139] B. S. Kerner and S. L. Klenov, J. Phys. A: Math. Theor. **43**, 425101 (2010).

[140] B. S. Kerner, German patent publications DE 000010308256A1, 2004; DE 102007008253A1, 2007; DE 102007008257A1, 2007; DE 102007008254A1, 2008; USA patents US 20070150167A1, 2007; US 7451039B2, 2008.